Article

Developmental Cell

A Gradient of Glycolytic Activity Coordinates FGF and Wnt Signaling during Elongation of the Body Axis in Amniote Embryos

Graphical Abstract

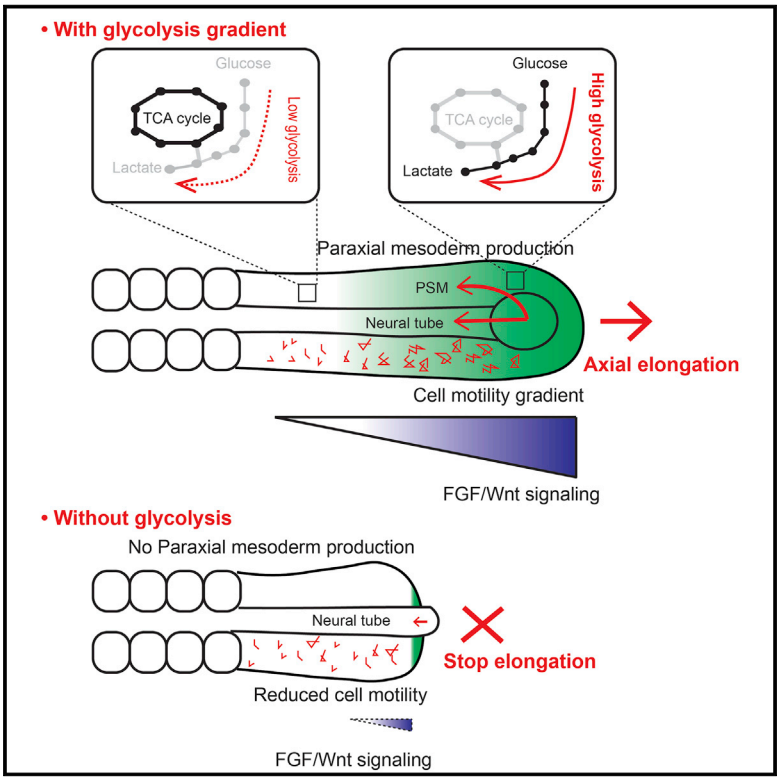

Highlights

- Identification of a glycolysis gradient in the embryo tail bud
- FGF signaling controls the transcription of glycolytic enzymes in the tail bud
- Glycolysis inhibition reduces cell motility and slows down axis elongation
- Glycolysis is required to maintain Wnt signaling and neuro-mesodermal fate

Authors

Masayuki Oginuma, Philippe Moncuquet, Fengzhu Xiong, Edward Karoly, Jérome Chal, Karine Guevorkian, Olivier Pourquié

Correspondence

pourquie@genetics.med.harvard.edu

In Brief

Mammalian embryos transiently exhibit aerobic glycolysis (Warburg effect). Oginuma and colleagues identify a glycolysis gradient in mouse and chick downstream of FGF in the amniote tail bud that controls posterior embryonic axis elongation. Glycolysis regulates presomitic mesoderm cell motility and Wnt signaling for specification of tail bud paraxial mesoderm fate.

Oginuma et al., 2017, Developmental Cell *40*, 342–353
February 27, 2017
http://dx.doi.org/10.1016/j.devcel.2017.02.001

CellPress

Developmental Cell
Article

A Gradient of Glycolytic Activity Coordinates FGF and Wnt Signaling during Elongation of the Body Axis in Amniote Embryos

Masayuki Oginuma,[1,2,3] Philippe Moncuquet,[1] Fengzhu Xiong,[2,3] Edward Karoly,[4] Jérome Chal,[1,2,3] Karine Guevorkian,[1,2,3] and Olivier Pourquié[1,2,3,5,*]

[1]Institut de Génétique et de Biologie Moléculaire et Cellulaire (IGBMC), CNRS (UMR 7104), Inserm U964, Université de Strasbourg, Illkirch 67400, France

[2]Department of Genetics, Harvard Medical School, Boston, MA 02115, USA

[3]Department of Pathology, Brigham and Women's Hospital, 60 Fenwood Road, Boston, MA 02115, USA

[4]Metabolon, 617 Davis Drive, Suite 400, Morrisville, NC 27560, USA

[5]Lead Contact

*Correspondence: pourquie@genetics.med.harvard.edu

http://dx.doi.org/10.1016/j.devcel.2017.02.001

SUMMARY

Mammalian embryos transiently exhibit aerobic glycolysis (Warburg effect), a metabolic adaptation also observed in cancer cells. The role of this particular type of metabolism during vertebrate organogenesis is currently unknown. Here, we provide evidence for spatiotemporal regulation of glycolysis in the posterior region of mouse and chicken embryos. We show that a posterior glycolytic gradient is established in response to graded transcription of glycolytic enzymes downstream of fibroblast growth factor (FGF) signaling. We demonstrate that glycolysis controls posterior elongation of the embryonic axis by regulating cell motility in the presomitic mesoderm and by controlling specification of the paraxial mesoderm fate in the tail bud. Our results suggest that glycolysis in the tail bud coordinates Wnt and FGF signaling to promote elongation of the embryonic axis.

INTRODUCTION

Early studies in chicken and mouse embryos have established that energy metabolism is tightly regulated during development (Johnson et al., 2003; Spratt, 1948). The early mouse preimplantation embryo does not rely on glucose as its main source of energy but rather uses pyruvate and lactate to feed the tricarboxylic acid (TCA) cycle and produce ATP (Brinster, 1965). Around the time of implantation a major metabolic transition occurs, leading the embryo to increase glucose uptake and glycolytic activity (Clough and Whittingham, 1983; Shepard et al., 1997). Most of this glycolytic activity coexists with an active TCA cycle and oxidative phosphorylation and results in lactate production (Johnson et al., 2003), thus resembling the Warburg metabolism or aerobic glycolysis of cancer cells (Vander Heiden et al., 2009). Subsequently, this intense glycolytic activity of the embryo decreases during organogenesis while respiration becomes the major mode of energy production (Wales et al., 1995). Aerobic glycolysis has been proposed to play a role in sustaining the intense proliferative activity of cancer and embryonic cells (Papaconstantinou, 1967; Vander Heiden et al., 2009). In the mammalian embryo, however, downregulation of the glycolytic activity occurs during early organogenesis, when very high levels of proliferation are observed, thus questioning the role of this metabolic adaptation. To date, most studies of the metabolic status of vertebrate embryonic cells in vivo are based on metabolic tracing which can only provide crude spatial resolution. Recent studies, however, have shown that aerobic glycolysis can be regulated in a cell-type- and stage-specific manner as for instance in the developing retina, in osteoblasts, or in endothelial cells (Agathocleous et al., 2012; Esen et al., 2013; Moussaieff et al., 2015). This raises the possibility of an instructive role for this particular type of metabolism in development (Shyh-Chang et al., 2013).

Here we investigated the role and regulation of metabolism in patterning and morphogenesis using musculoskeletal development as a paradigm. Skeletal muscles and vertebrae derive from the paraxial mesoderm, which is continuously produced by gastrulation first in the primitive streak and then in the tail bud. Newly generated paraxial mesoderm appears as bilateral strips of mesenchyme called presomitic mesoderm (PSM), which periodically segment to generate the embryonic somites (Hubaud and Pourquie, 2014). Somites provide the blueprint for the metameric arrangement of vertebrae and associated muscles. Periodic somite formation is driven by a molecular oscillator, termed the segmentation clock, which drives rhythmic activation of the Wnt, fibroblast growth factor (FGF), and Notch pathways in the PSM (Hubaud and Pourquie, 2014). The segmental response to the oscillator is gated to a specific level of PSM called the determination front by a system of traveling posterior-to-anterior gradients of Wnt and FGF signaling. Cells of the PSM exhibit a gradient of random motility (cell diffusion) controlled by FGF, which has been proposed to control the posterior elongation movements involved in body axis formation (Benazeraf et al., 2010). In the paraxial mesoderm, the differentiation process is associated with a striking modular compartmentalization of

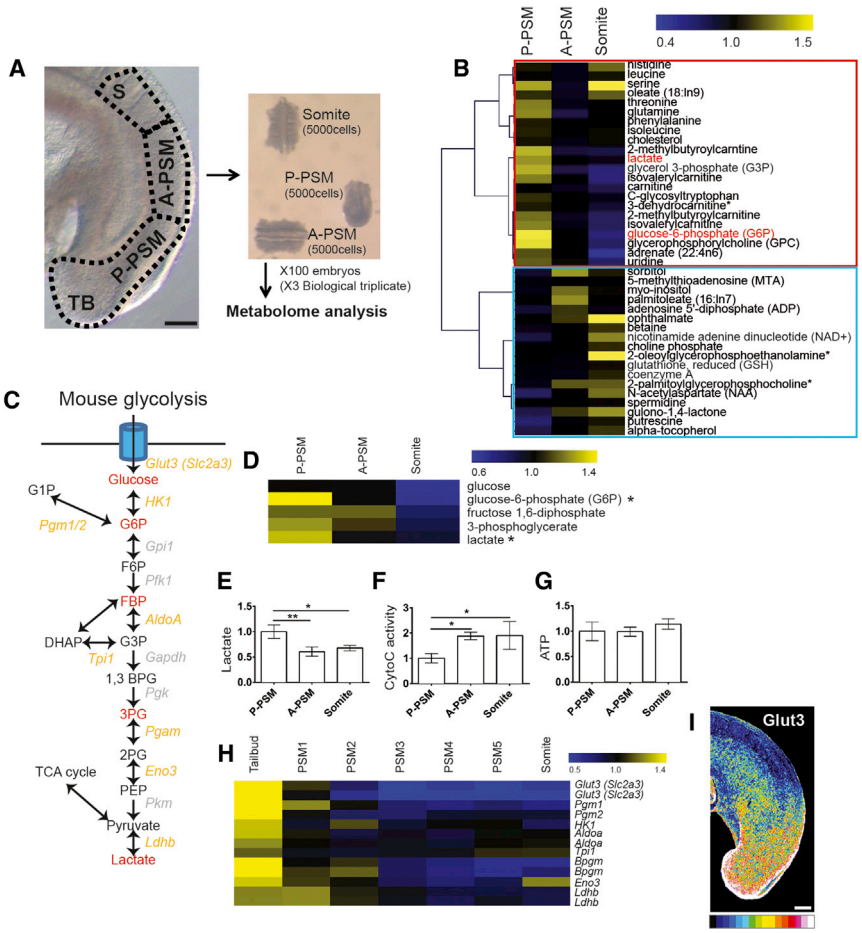

Figure 1. A Posterior Glycolytic Gradient in the Mouse Tail Bud

(A) Lateral view of the posterior region of E9.5 mouse embryo showing the three domains used for metabolomics analysis. TB, tail bud; S, somite; A-PSM and P-PSM, anterior and posterior presomitic mesoderm, respectively. Each domain contains approximately 5,000 cells. Scale bar, 100 μm.

(B) Clustering analysis of the 39 metabolites showing the most significant differential expression along the posterior region of the embryo. Color bar shows fold change from mean. Red box highlights downregulated metabolites and blue box upregulated metabolites during differentiation.

(C) Schematic representation of the mouse glycolytic cascade. Red labeling indicates metabolites detected in the metabolomics analysis. Yellow labeling indicates the glycolytic enzyme transcripts downregulated in the mouse embryo tail bud and PSMs. Gray labeling indicates the glycolytic enzyme transcripts that are not detected or not changed in the mouse embryo tail bud and PSMs.

(D) Expression profiles of the metabolites associated to glycolysis detected in the metabolomics analysis (*$p < 0.05$ by t test). The color bar shows fold change from mean of all triplicate samples.

(E–G) Enzymatic detection of relative lactate levels (E), cytochrome *c* oxidase activity (F), and relative ATP concentrations (G) during tail bud differentiation. Graphs show triplicate experiments. Values were normalized by P-PSM. Error bars denote ±SD. Statistical significance was assessed with one-way ANOVA followed by Tukey's test: *$p < 0.05$, **$p < 0.01$.

(H) Expression profiles of transcripts coding for glycolytic enzymes downregulated in the mouse PSM during differentiation. Each value is normalized to the mean of MAS values of all triplicate mouse microarray series. The color bar shows fold change from mean.

(I) Lateral view of the tail bud region of 9.5-day-old mouse embryo stained with an antibody against Glut3 (n = 5). Maximum projection of confocal sections. Fluorescence intensity is shown by pseudocolor image (16 colors) using ImageJ. Higher levels of Glut3 proteins are indicated in red-yellow. Scale bar, 100 μm. See also Figure S1; Tables S1 and S2.

the transcription of essential components of translation and oxidative metabolism, which become upregulated as cells differentiate (Ozbudak et al., 2010). Furthermore, hypoxia can downregulate FGF signaling in the paraxial mesoderm, leading to an arrest of the segmentation clock and ultimately to vertebral defects (Sparrow et al., 2012). These observations support a crosstalk between signaling and metabolism and argue for a dynamic regulation of metabolism during paraxial mesoderm development.

In this report, combining metabolomic and transcriptomic approaches we identify a posterior-to-anterior gradient of glucose uptake and glycolysis in the tail bud region of the mouse and chicken embryos. We show that the tail bud glycolytic gradient is established in response to graded transcription of rate-limiting glycolytic enzymes downstream of FGF signaling. Inhibiting glycolysis in the chicken embryo leads to an arrest of axis elongation associated with increased extracellular pH and decreased cell motility in the posterior PSM. The elongation arrest is also accompanied by premature differentiation of the SOX2-BRACHYURY double-positive neuro-mesodermal precursors (NMPs) toward a neural fate, resulting from inhibition of Wnt signaling in the tail bud. Thus our work identifies a striking role for glycolysis in integrating cell signaling during body axis formation.

RESULTS AND DISCUSSION

Identification of a Posterior Gradient of Glycolysis in the Mouse Tail Bud

To explore the regulation of metabolism during paraxial mesoderm differentiation, we performed a comprehensive metabolomic analysis of the developing posterior body axis in mouse embryos. To this end, we dissected the posterior part of 300 embryonic day 9.5 (E9.5) into three adjacent domains corresponding to the progressively more differentiated levels of the posterior PSM (P-PSM) including the tail bud, anterior PSM (A-PSM), and newly formed somites (Figure 1A). The relative abundance of a set of 2,400 metabolites was analyzed for each sample by liquid chromatography-tandem mass spectrometry (LC-MS/MS) and gas chromatography-mass spectrometry (GC-MS). This strategy identified a total of 129 metabolites that were reliably detected in the embryo samples (Figure S1A and Table S1). Thirty-nine of these metabolites showed statistically significant

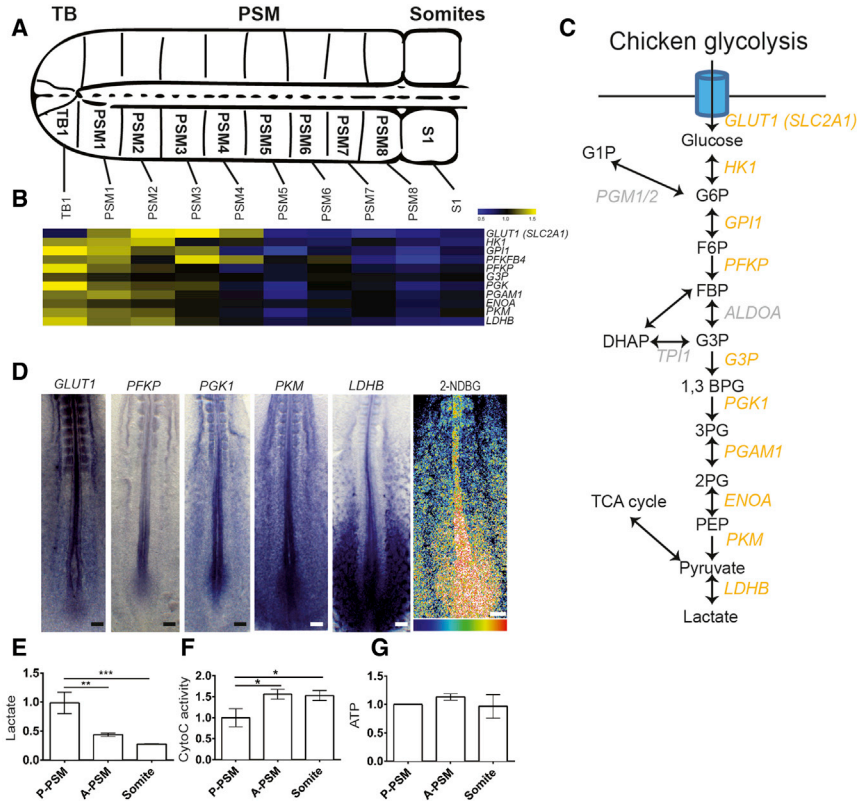

Figure 2. Conservation of the Posterior Glycolytic Gradient in the Chicken Embryo

(A) Schematic representation of the posterior portion of a 2-day-old chicken embryo. The fragments microdissected to generate the microarray series are indicated. Dorsal view, anterior to the right. TB, tail bud; PSM, presomitic mesoderm.

(B) Expression profiles of transcripts coding for glycolytic enzymes downregulated in chicken PSM during differentiation as detected in the microarray series. Each value is normalized to the mean of MAS values of all duplicate chicken microarray series. Color bar shows fold change from mean.

(C) Schematic representation of the chicken glycolytic cascade. Yellow labeling indicates the glycolytic enzymes whose transcripts are downregulated in the chicken embryo tail bud and PSM. Gray labeling indicates the glycolytic enzyme transcripts that are not detected or not changed in the mouse embryo tail bud and PSMs.

(D) Left: posterior region of 2-day-old chicken embryos hybridized with probes for the glucose transporter *GLUT1*, and for the glycolytic enzymes *PFKP*, *PGK1*, *PKM*, and *LDHB*. Right: fluorescent glucose (2-NDBG) uptake in the posterior region of a 2-day-old chicken embryo (n = 11). Maximum projection of confocal sections. Fluorescence intensity is shown by pseudocolor image (16 colors) using ImageJ. Higher levels of fluorescent 2-NDBG are indicated in red-yellow. Ventral view, anterior to the top. Scale bar, 100 μm.

(E–G) Enzymatic detection of relative lactate level (E), cytochrome *c* oxidase activity (F), and relative ATP concentration (G) during tail bud differentiation. Graphs represent triplicate experiments. Values were normalized by the P-PSM. Error bars denote ±SD. Statistical significance was assessed with one-way ANOVA followed by Tukey's test: *p < 0.05, **p < 0.01, ***p < 0.001.

See also Figure S2 and Table S3.

variation during differentiation (Figure 1B and Table S1). Several metabolites involved in glycolysis, such as lactate or glucose-6-phosphate (G6P), were detected at significantly higher levels (1.35- and 1.49-fold respectively, $p < 0.05$) in P-PSM compared with A-PSM (Figures 1B–1D and S1B; Table S1). Other glycolytic metabolites including glucose, fructose-1,6-diphosphate (FBP), and 3-phosphoglycerate (3-PG) also exhibited trends suggesting enrichment in the P-PSM (Figures 1C, 1D, and S1B; Table S1). Other important nutrients such as glutamine also showed a similar posterior gradient (Figures 1B and S1B). Using an enzymatic assay, we found significantly higher lactate levels in the P-PSM and tail bud, compared with A-PSM and somites (Figure 1E), consistent with more active glycolysis in more posterior regions. We also found that cytochrome *c* oxidase activity was increased in A-PSM and somite but was still detected in the posterior region experiencing high glycolytic activity (Figure 1F). Cytochrome *c* oxidase activity forms a gradient opposite to that of glycolysis, consistent with the increased regulation of translation and oxidative metabolism reported in the zebrafish anterior PSM (Ozbudak et al., 2010). This supports the notion that glycolysis plays a more important role than respiration in the posterior part of the embryo. We did not detect any significant difference in ATP concentration along the PSM (Figure 1G). We next analyzed the expression of key glycolytic enzymes in a previously generated PSM microarray series of consecutive microdissected fragments spanning the entire PSM in E9.5 mouse embryos (Chal et al., 2015). Transcripts coding for *Phosphoglucomutase* (*Pgm1/2*), *Hexokinase* (*HK1*), *Aldolase* (*AldoA*), *Triose phosphate isomerase* (*Tpi1*), *2,3-Phosphoglycerate mutase* (*Bpgm*), *Enolase* (*Eno3*), and *Lactate dehydrogenase* (*Ldhb*) are enriched at the level of the tail bud/posteriormost PSM and show a posterior expression gradient (Figure 1H and Table S2). Glucose transporter 3 (Glut3 or Slc2a3), which controls entry of glucose into the cell, also showed graded expression in the PSM and the tail bud at the mRNA and at the protein level (Figures 1H and 1I; Table S2). Together, these observations identify a gradient of glycolytic activity associated with graded transcription of glycolytic enzymes in the posterior PSM and tail bud of mouse embryos.

Conservation of the Posterior Glycolytic Gradient in Developing Chicken Embryos

We next investigated whether this graded glycolytic activity is conserved between mouse and chicken embryos. We generated a microarray series from consecutive fragments of the developing chicken PSM similar to that performed in mouse (Chal et al., 2015) (Figures 2A and S2). Most genes coding for glycolytic enzymes showed a posterior expression gradient in the chicken microarray series (Figures 2A–2C and Table S3). Graded expression of several glycolytic enzymes was confirmed by in situ hybridization (Figure 2D). The glucose transporter *GLUT3* was not detected in the chicken PSM, but *GLUT1* (*SLC2A1*) showed a

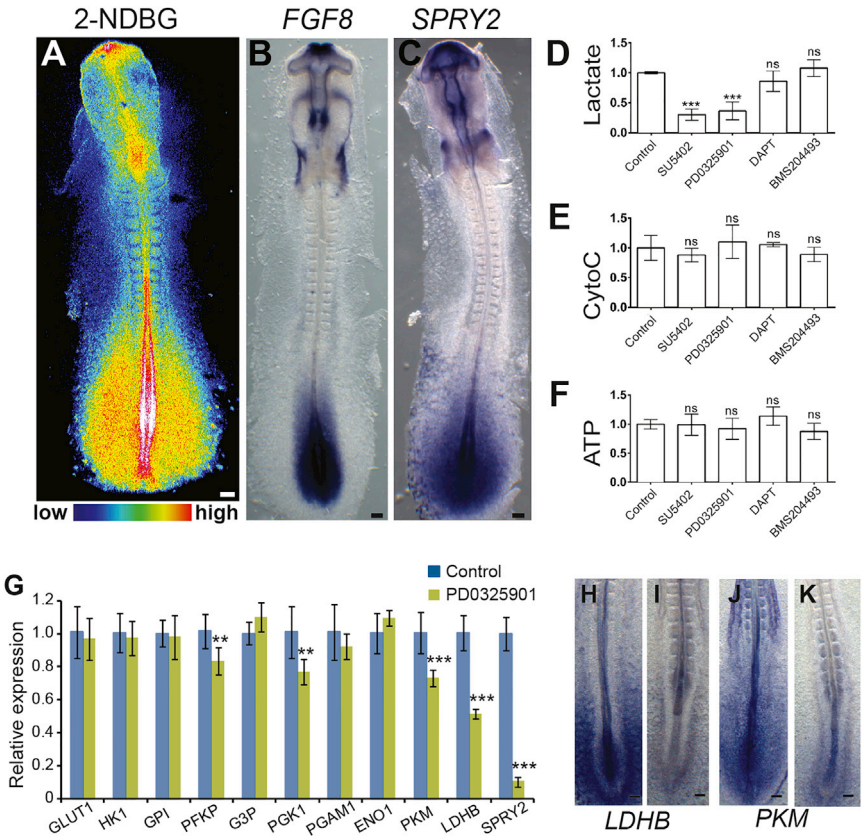

Figure 3. FGF Signaling Regulates Glycolysis in the Posterior Part of the Embryo

(A) Fluorescent glucose (2-NDBG) uptake in a 2-day-old chicken embryo. Maximum projection of confocal sections. Fluorescence intensity is shown by pseudocolor image (16 colors) using ImageJ. Higher levels of uptake are indicated in red-yellow. Dorsal view, anterior to the top. Scale bar, 100 μm.

(B and C) Whole-mount in situ hybridization of 2-day-old chicken embryos with *FGF8* (B) and *SPRY2* (C) probes. Dorsal view, anterior to the top. Scale bar, 100 μm.

(D–F) Enzymatic detection of relative lactate level (D), cytochrome *c* oxidase activity (E), and of relative ATP concentration (F) in the posterior part of 2-day-old chicken embryos treated with inhibitors of FGF (SU5402), MAPK (PD0325901), Notch (DAPT), and retinoic acid (BMS204493) (n = 6 for each condition). Graphs represent triplicate experiments. Values are normalized by untreated control embryos. Error bars denote ±SD. Statistical significance was assessed with one-way ANOVA followed by Tukey's test: ***$p < 0.001$; ns (not significant, $p > 0.05$).

(G) qPCR analysis of glycolytic enzymes expression levels in control (blue) and in embryos treated with the MAPK inhibitor PD0325901 (green). Graphs represent triplicate experiments. Values are normalized by untreated control embryos, Error bars denote ±SD. Statistical significance was assessed with unpaired two-tailed Student's t test: **$p < 0.01$, ***$p < 0.001$.

(H–K) Whole-mount in situ hybridization with probes for the rate-limiting glycolytic enzymes *LDHB* (H, n = 8; I, n = 7) and *PKM* (J, n = 8; K, n = 8), in control (H and J) and PD0325901-treated (I and K) 2-day-old chicken embryos. Ventral view, anterior to the top. Scale bar, 100 μm.

posterior expression gradient (Figures 2B–2D and Table S3). Furthermore, glucose uptake analysis with fluorescent glucose (2-NDBG) (Itoh et al., 2004; Yoshioka et al., 1996) demonstrated a clear posterior gradient peaking in the tail bud (Figure 2D). While this is not a direct measure of glucose uptake, because the fluorophore on this molecule is much larger than glucose, it is expected to show some correlation with glucose uptake. 2-NDBG most likely interacts with glucose transporters and is a surrogate for glucose transporter expression. In the chicken embryo, analysis of lactate production using an enzymatic assay also shows a posterior gradient (Figure 2E). As observed in mouse, cytochrome *c* oxidase activity is also detected in the posterior glycolytic regions, and increased in A-PSM and somite (Figure 2F). No significant difference in ATP concentration was observed along the anterior-posterior axis (Figure 2G). Thus, the posterior-to-anterior gradient of glycolytic activity in the tail bud is conserved between mouse and chicken embryos.

FGF Signaling Regulates the Transcription of Rate-Limiting Glycolytic Enzymes

High levels of glycolysis have often been associated with the need to produce important quantities of substrates for anabolic reactions required to sustain the rapid proliferation of cancer or embryonic cells (Vander Heiden et al., 2009). The proliferation rate and cell-cycle length in the tail bud and the somite region have been measured using a variety of approaches and were found to remain relatively stable in the 2-day-old chicken embryo with a duration of around 9–11 hr (Gomez et al., 2008; Primmett et al., 1989; Venters et al., 2008). Therefore, the spatiotemporal regulation of glycolysis in the trunk is unlikely to reflect changes in the proliferation regime of embryonic cells. In the 2-day-old chicken embryo, fluorescent glucose uptake is strikingly regionalized, peaking in the tail bud, posterior PSM, and neural tube, the forming limb buds, the rhombomere 4 region, and the anterior neural ridge, which are regions that largely overlap with regions where *FGF8* and its target *SPRY2* are expressed (Figures 3A–3C). In the posterior region of the embryo, the gradient of glucose uptake and glycolytic activity is parallel to the gradient of FGF signaling, which controls segmentation and elongation of the body axis (Benazeraf and Pourquie, 2013). To investigate the interactions between FGF signaling and the regulation of glycolysis, we examined the metabolic activity following treatment with FGF/mitogen-activated protein kinase (MAPK) inhibitors (Figures 3D–3F). Lactate production was inhibited following treatment with SU5402 (an FGFR1 inhibitor) and PD0325901 (a MAPK inhibitor) (Figure 3D). In contrast, these inhibitors had no effect on mitochondrial cytochrome *c* oxidase activity or ATP concentration (Figures 3E and 3F). Inhibitors of other signaling pathways important for PSM patterning including Notch (DAPT) and retinoic acid (BMS204493) did not affect lactate, ATP concentration, or cytochrome *c* oxidase function (Figures 3D–3F). Significant downregulation of the expression of genes

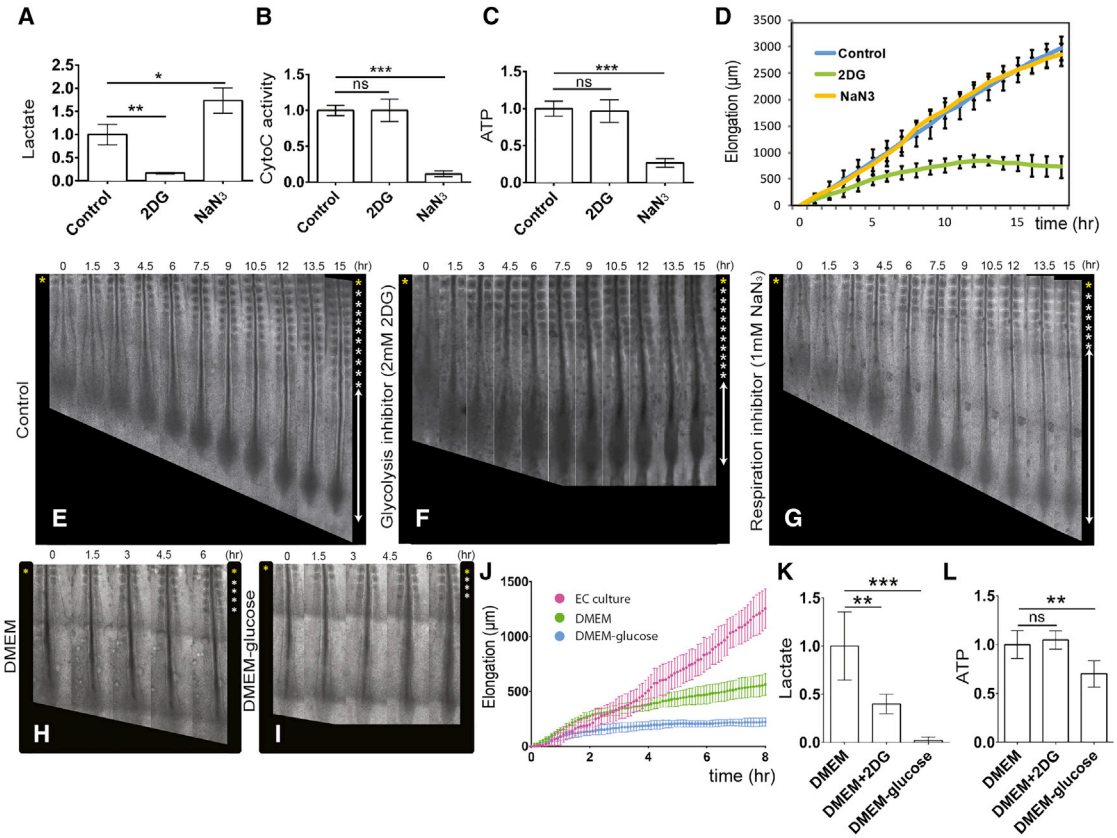

Figure 4. Glycolysis Controls Posterior Elongation of the Embryonic Axis

(A–C) Enzymatic detection of relative lactate level (A), cytochrome *c* oxidase activity (B), and relative ATP concentration (C) in the posterior region of control 2-day-old chicken embryos and in embryos treated with 2DG or NaN_3 (n = 6 embryos for each condition). Graphs represent triplicate experiments. Values are normalized by untreated control embryos. Error bars denote ±SD. Statistical significance was assessed with one-way ANOVA followed by Tukey's test: *$p < 0.05$, **$p < 0.01$, ***$p < 0.001$; ns (not significant), $p > 0.5$.

(D) Increase in axis length (elongation) measured over time using time-lapse microscopy (mean ± SD). Blue, control embryos (n = 8); green, 2DG-treated embryos (n = 7); yellow, NaN_3-treated embryos (n = 5).

(E–G) Elongation time course in a control (E), 2DG-treated (F), and NaN_3-treated (G) 2-day-old chicken embryo. Bright-field micrographs of the posterior region of a chicken embryos taken at 1.5-hr intervals. Somites formed at the last time point are indicated by asterisks on the right. Ventral views, anterior to the top. See also Movie S1.

(H and I) Elongation time course in chemically defined DMEM-based culture with 0.15% glucose (DMEM) (H) and without glucose (DMEM-glucose) (I). Bright-field micrographs of the posterior region of 2-day-old chicken embryos taken at 1.5-hr intervals. Somites formed at the last time point are indicated by asterisks on the right. Ventral views, anterior to the top.

(J) Increase in axis length (elongation) measured over time using time-lapse microscopy (mean ± SD). Magenta, embryos in control EC culture (n = 5); green, embryos in defined 0.15% glucose DMEM-based cultures (n = 4); blue, embryos in defined DMEM-based culture without glucose (n = 5).

(K and L) Enzymatic detection of relative lactate level (K) and relative ATP concentration (L) in the posterior region of control 2-day-old chicken embryos and in embryos cultured in defined DMEM-based medium with or without 0.15% glucose and in 2DG-treated embryos (n = 4 embryos for each condition). Graphs represent quadruple experiments. Values are normalized to DMEM 0.15% glucose embryos. Error bars denote ±SD. Statistical significance was assessed with one-way ANOVA followed by Tukey's test: **$p < 0.01$, ***$p < 0.001$; ns (not significant), $p > 0.5$.

See also Figure S3.

coding for the rate-limiting glycolytic enzymes: *PFKP*, *PGK1*, *PKM*, and *LDHB* (0.83-, 0.77-, 0.73-, and 0.52-fold, respectively; $p < 0.01$) was observed by qPCR after PD0325901 treatment compared with control untreated embryos (Figure 3G). Downregulation of this subset of glycolytic enzymes after PD0325901 treatment was subsequently confirmed by in situ hybridization (Figures 3H–3K; data not shown). These results suggest that the posterior gradient of FGF/MAPK signaling controls the high glycolytic activity in the posterior PSM/tail bud by regulating the transcription of rate-limiting glycolytic enzymes.

Glycolysis Regulates Body Axis Elongation, Extracellular pH, and Cell Motility

To explore the role of glycolysis in tail bud development, we analyzed the effect of 2-deoxy-D-glucose (2DG), a competitive inhibitor of hexokinase, on stage 9–10 Hamburger and Hamilton (HH) (Hamburger and Hamilton, 1992) chicken embryos cultured in vitro using the Early Chick (EC) culture system (Chapman et al., 2001). 2DG treatment led to strong downregulation of lactate production (Figure 4A), but not of cytochrome *c* oxidase activity in the embryo (Figure 4B). ATP concentration was not

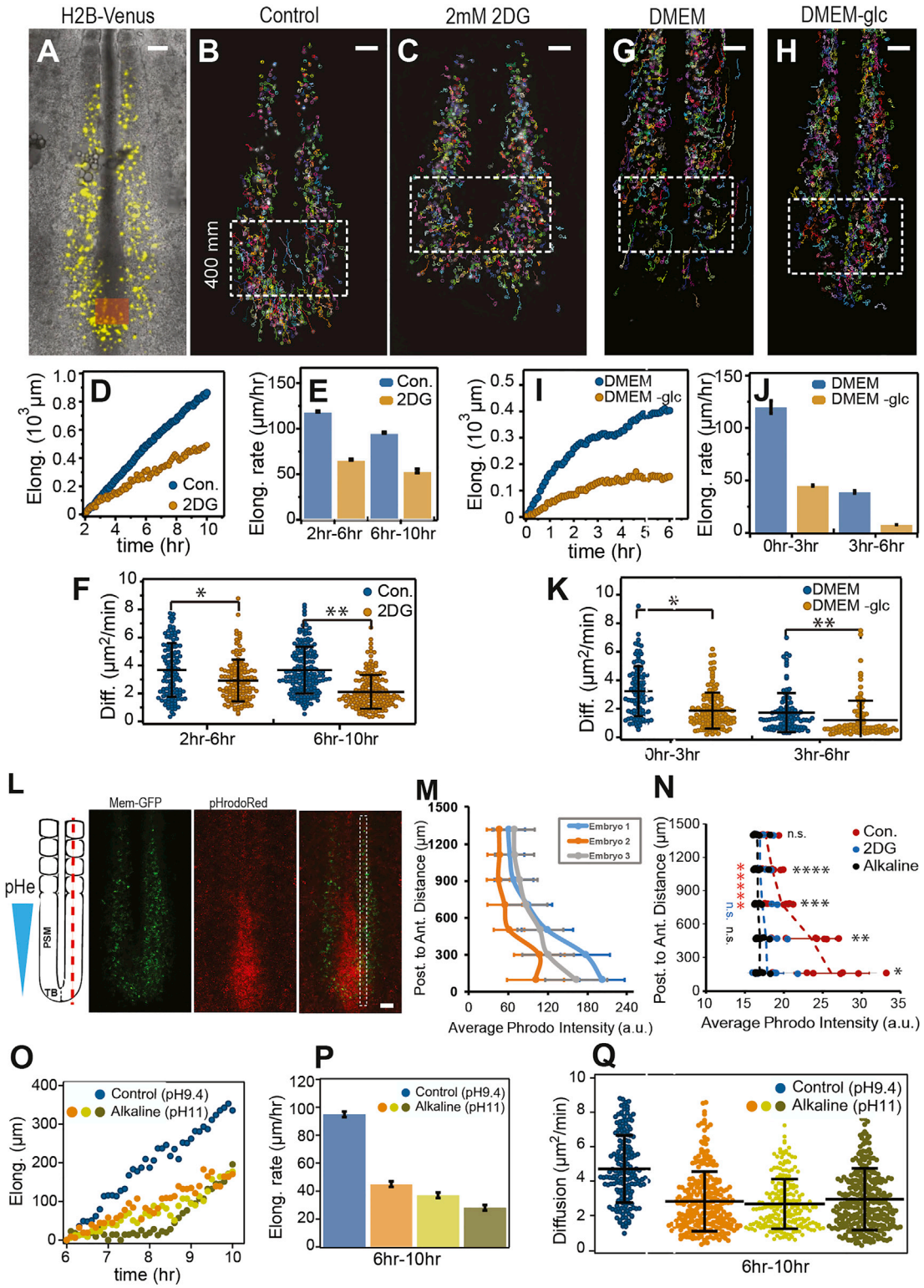

Figure 5. Glycolysis Inhibition Decreases Cell Motility and Increases pH in the Posterior PSM

(A–F) Effect of 2DG treatment on cell motility (diffusion) and PSM elongation in 2-day-old chicken embryos. (A) Electroporated PSM cells expressing H2B-Venus are shown in yellow. (B and C) PSM cell trajectories for control and 2DG-treated embryos, respectively. Only tracks of cells located in the posterior PSM inside the box were used in the analysis. Scale bars, 100 µm. (D) Elongation curves showing the posterior displacement of the tail bud (orange box) as a function of time in

(legend continued on next page)

significantly changed upon 2DG treatment suggesting that glycolysis in the posterior PSM/tail bud plays a limited role in energy production (Figure 4C). In contrast, treating chicken embryos with the respiration inhibitor sodium azide (NaN_3) increased lactate production while it effectively (albeit incompletely) decreased cytochrome *c* oxidase activity and ATP concentration in the tail bud region of the embryo (Figures 4A–4C). 2DG treatment severely affected axis elongation, generating truncated embryos, whereas somite formation continued at a normal pace, leading to a progressive shortening of PSM length (Figures 4D–4F and Movie S1). In contrast, axis elongation was not affected by sodium azide treatment, while somite segmentation was blocked (Figures 4D and 4G; Movie S1), indicating a specific requirement of glycolysis for axial elongation. We next established a chemically defined culture system for chicken embryos in which we can control the level of energy substrates. When embryos were cultured in medium containing 0.15% glucose, elongation proceeded normally, albeit at a slower pace compared with control EC cultures (Figures 4H and 4J). In embryos cultured for 3–6 hr in the same medium but devoid of glucose, elongation was around 4-times slower when compared with embryos cultured in glucose-containing medium (Figures 4I and 4J). In embryos cultured in glucose-free medium, a strong downregulation of lactate production accompanied by a slight but significant decrease of ATP concentration was observed in the posterior region (Figures 4K and 4L). No significant effect on cell proliferation or cell death was observed in embryos cultured in glucose-free medium after 3 hr (Figure S3). To explore the role of glutamine, which exhibits a gradient parallel to the glycolytic metabolites, we cultured embryos in glutamine-free defined medium. Under these conditions, elongation proceeded similarly to glutamine-containing controls (data not shown). Thus, glutamine cannot substitute to glucose to promote elongation of the posterior body axis.

A gradient of random cell motility (diffusion) controlled by FGF/MAPK signaling in the PSM has been proposed to drive posterior elongation movements in the chicken embryo (Benazeraf et al., 2010). To test whether glycolysis controls motility in the posterior PSM, we measured the diffusion and analyzed trajectories of posterior PSM cells labeled by electroporation with H2B-Venus in embryos treated or not with 2DG (Figures 5A–5C and Movie S2). We showed that inhibition of glycolysis leads to a progressive downregulation of cell diffusion, which correlates with the slowing down of elongation (Figures 5D–5F). We observed a similar reduction of cell diffusion in embryos electroporated with H2B-Venus cultured in the chemically defined glucose-free medium when compared with control embryos (Figures 5G–5K and Movie S3).

In tumors or blastocyst embryos, cell motility is promoted by aerobic glycolysis, which leads to acidification of the extracellular environment as a result of lactic acid excretion (Gardner, 2015; Parks et al., 2013). This in turn triggers activation of matrix metalloproteinases (MMP) involved in remodeling extracellular matrix. In the PSM, the pH sensitive enzyme MMP2 is expressed in a posterior gradient (Figures S4A and S4B). We observed that 2-day-old chicken embryos labeled with the pH sensor pHrodo Red (Ogawa et al., 2010) exhibit a posterior-to-anterior gradient of extracellular pH, with the lowest pH found in the tail bud where glycolysis is most active (Figures 5L and 5M). This pH gradient can be abolished by incubating embryos on alkaline plates (pH 11) (Figure 5N). Treatment of the embryos with 2DG prior to labeling also results in a uniformly higher pH (Figure 5N), suggesting that glycolysis is involved in the acidification of the extracellular environment at the posterior end of the embryo. Embryos cultured on alkaline plates also exhibit much slower axis elongation (Figure 5O) while somite formation continues to proceed at a normal pace (Figures S4C and S4D; Movie S4). Paraxial mesoderm markers such as *CMESO1* or *T* were still expressed in embryos cultured on alkaline plates (Figures S4E–S4H). Analysis of embryos in which paraxial mesoderm precursors were electroporated with an H2B-Venus construct cultured on alkaline plates revealed a decrease in cell diffusion paralleling the decrease in the speed of axis elongation (Figures 5O–5Q and Movie S4). Together, these experiments suggest that glycolysis acts downstream of FGF signaling to promote acidification of the extracellular environment and cell motility.

the wild-type and 2DG-treated embryos. (E) Elongation rates of the embryos shown in (D); error bars denote ±SD of the linear adjustments to data in (D). (F) Cell diffusion for control and 2DG-treated embryos shown from 2 to 6 hr and from 6 to 10 hr (mean ± SD, *p = 0.0004, **p < .0001, t test). See also Movie S2.

(G–K) Cell motility (diffusion) and PSM elongation in chemically controlled conditions. (G and H) PSM cell trajectories for 2-day-old chicken embryos cultured in DMEM and DMEM without glucose, respectively. Only tracks of cells located in the posterior PSM inside the box are used in the analysis. Scale bars, 100 μm. (I) Elongation curves showing the posterior displacement of the tail bud as a function of time in the DMEM and DMEM without glucose conditions. (J) Elongation rates of the embryos shown in (I); error bars denote ±SD of the linear adjustments to data in (I). (K) Cell diffusion for DMEM and DMEM without glucose conditions shown from 0 to 3 hr and from 3 to 6 hr (mean ± SD, *p < 0.00001, **p = 0.0069, t test). See also Movie S3.

(L) Extracellular pH in the posterior part of a 2-day-old chicken embryo labeled with pHrodo red showing the gradient of extracellular pH (pHe). Red fluorescence labels regions of lower pH. Electroporated PSM cells expressing MEM-GFP are shown in green (Okada et al., 1999). Maximum projection of confocal sections of a 2-day-old chicken embryo. Ventral views, anterior to the top. pHrodo intensity was measured specifically in the PSM in the region highlighted by a white dashed box. Scale bar, 100 μm.

(M) Quantification of intensity of pHrodo red. pHrodo Intensity measured in three different embryos along the posterior-anterior axis using stripes in PSM as described in (L). Measurements were binned every 200 μm and the average intensity (±SD) is shown. Absolute pHrodo intensity values may vary as a result of different embryo/imaging conditions. Embryo 1 is (L).

(N) Effect of culturing embryos on 2DG-containing and alkaline plates on the pHe gradient. Each dot represents average fluorescence intensity measured in a ~0.26-mm^2 area of each embryo along the posterior-anterior axis. Lines represent average intensity (±SD) (control, n = 7; alkaline, n = 8; 2DG, n = 7). *p = 0.001, **p = 0.001, ***p = 0.003, ****p = 0.006; n.s. (not significant), p = 0.15 (t tests). ****p = 0.002 (red, control); n.s. (blue, 2DG), p = 0.14; n.s. (black, NaOH), p = 0.35. Paired t tests compared the anterior-posterior ends of the pHe gradient.

(O–Q) Effect of culture on alkaline plates on cell motility and PSM elongation in 2-day-old chicken embryos. (O) Elongation curves for control and embryos cultured on alkaline plates. (P) Elongation rate corresponding to the curves in (O). (Q) Cell diffusion for control and embryos cultured on alkaline plates (mean ± SD, p < 0.01 between control and alkaline plates and not significant among alkaline plates using one-way ANOVA followed by Tukey's test).

See also Movie S4 and Figure S4.

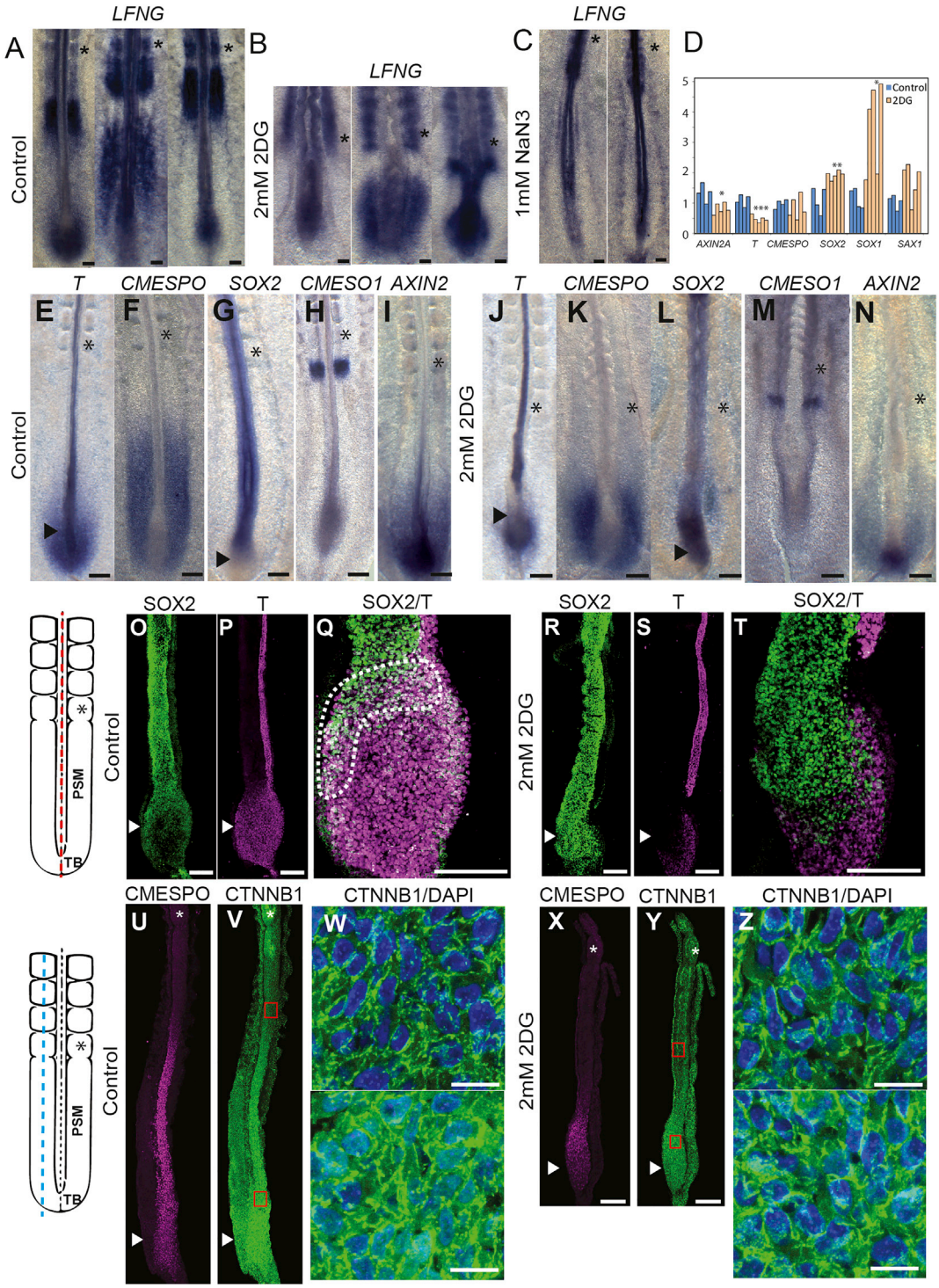

Figure 6. Inhibition of Glycolysis Phenocopies Wnt Signaling Inhibition in the Tail Bud

(A–C) Whole-mount in situ hybridizations showing the posterior region of 2-day-old control (A, n = 24), 2DG-treated (B, n = 16), and NaN_3-treated (C, n = 13) chicken embryos hybridized with *LFNG* probe. Asterisk indicates newly formed somites.

(D) qPCR analysis of the posterior region of 2-day-old chicken embryos treated or not with 2DG and incubated for 10 hr. Values are normalized to the mean of control embryos. Each bar represents one embryo. Statistical significance was assessed with unpaired two-tailed Student's t test. *$p < 0.05$, **$p < 0.01$, ***$p < 0.001$.

(E–N) Whole-mount in situ hybridizations showing the posterior region of 2-day-old control (E–I) or 2DG-treated (J–N) chicken embryos hybridized with the following probes: *T* (*BRACHYURY*) (E, n = 4; J, n = 6); *CMESPO* (F, n = 5; K, n = 5); *SOX2* (G, n = 7; L, n = 4); *CMESO1* (H, n = 5; M, n = 4); *AXIN2* (I, n = 5; N, n = 4). Asterisks indicate the last formed somite and arrowheads indicate the tail bud region. Ventral view, anterior to the top.

(legend continued on next page)

Glycolysis Regulates Wnt Signaling and Maintenance of the NMPs in the Tail Bud

Rhythmic somite formation is driven by a molecular oscillator, termed the segmentation clock, which drives cyclic activation of the Wnt, FGF, and Notch pathways (Hubaud and Pourquie, 2014). Dynamic patterns of *Lunatic Fringe (LFNG)*, a cyclic gene controlled by the segmentation clock, were observed in 2DG-treated embryos, suggesting that periodic signaling driven by the clock remains functional (Figures 6A and 6B). This contrasts with data obtained on PSM explants from mouse embryos cultured in absence of glucose, where *Lunatic Fringe* periodic expression was blocked (Bulusu et al., 2017 [this issue of *Developmental Cell*]). The two sets of experiments, however, differ in that 2DG inhibition of glycolysis is incomplete (Figure 4A). In the chicken embryo, the presumptive segment is first visible as a stripe of expression of the gene *CMESO1* (a chicken homolog of the mouse *Mesp2* gene). Upon 2DG treatment, *CMESO1* mRNA expression was normally expressed as a bilateral stripe in the anterior PSM (Figures 6H and 6M). In contrast, expression of *Lunatic Fringe* was downregulated in presence of NaN_3, consistent with the segmentation defects observed (Figure 6C). Accordingly, exposing developing mouse embryos to hypoxic conditions disrupts FGF signaling and segmentation (Sparrow et al., 2012). Thus, 2DG treatment impairs body elongation but not segmentation.

Maintenance of the posterior elongation movements requires a constant supply of motile cells in the forming posterior PSM (Benazeraf and Pourquie, 2013). In 2DG-treated embryos, the size of the expression domains of the posterior PSM markers, *T/BRACHYURY* (Figures 6E and 6J) and *CMESPO* (the chicken homolog of *Mesogenin1*) (Figures 6F and 6K) strongly decreased, suggesting an arrest of PSM cell production. In contrast, expression of the neural marker *SOX2* was expanded posteriorly in the tail bud of treated embryos (Figures 6G and 6L). No significant effect of 2DG treatment on proliferation and apoptosis in the paraxial mesoderm could be detected (Figure S5). The posterior paraxial mesoderm and neural tube derive from a group of NMPs found in the tail bud region, which co-express SOX2 and BRACHYURY (Henrique et al., 2015; Kimelman, 2016; Tzouanacou et al., 2009) (Figures 4O–4Q). In chicken embryos treated with 2DG, the SOX2-BRACHYURY double-positive expression domain was replaced by cells only expressing SOX2 (compare Figures 6O–6Q with 6R–6T). This suggests that NMPs differentiated into neural cells, leading to the termination of paraxial mesoderm production. We electroporated the NMP region in the anterior primitive streak with an H2B-RFP construct in transgenic chicken embryos expressing GFP ubiquitously and monitored the fate of the descendants of the electroporated NMPs. In control embryos, NMPs contribute to both neural and paraxial mesoderm lineages whereas in embryos treated with 2DG, NMPs stop producing paraxial mesoderm cells while continuing to populate the forming neural tube (Movie S5). Since axis elongation is largely driven by the posterior paraxial mesoderm (Benazeraf et al., 2010), the arrest of its production can contribute to explaining the arrest of elongation. Therefore, the high glycolytic state in the tail bud is also required for the maintenance of the NMP cells and the regulation of the balance of the differentiation rate between paraxial mesoderm and neural lineages. This phenotype resembles that observed when either *Wnt3a* or its targets *Brachyury* and *Tbx6* are mutated in mouse where ectopic neural tissue forms instead of paraxial mesoderm (Chapman and Papaioannou, 1998; Greco et al., 1996; Nowotschin et al., 2012; Takemoto et al., 2011; Yamaguchi et al., 1999). In the chicken embryo, the termination of axis elongation is also associated with a decrease in Wnt signaling and the differentiation of the $SOX2^+$/$BRACHYURY^+$ cells into $SOX2^+$/$BRACHYURY^-$ cells (Olivera-Martinez et al., 2012). Thus, the phenotype elicited by 2DG treatment phenocopies Wnt loss of function in the tail bud of mouse and chicken embryos. This led us to examine whether glycolysis inhibition downregulates Wnt signaling. In control chicken embryos, nuclear β-catenin (CTNNB1) shows a posterior gradient in the PSM as reported for mouse embryos (Figures 6U–6W) (Aulehla et al., 2008). This high nuclear β-catenin domain coincides with the expression domain of *CMESPO* (Figure 6U), a direct target of Wnt signaling in the PSM (Buchberger et al., 2000; Wittler et al., 2007). 2DG treatment strongly reduced nuclear β-catenin localization in the posterior PSM region (Figures 6X–6Z). By qPCR on 2DG-treated embryos' posterior domain, we detected a significant downregulation of the Wnt targets *AXIN2* and *BRACHYURY*, whereas the neural markers *SOX2* and *SOX1* were significantly upregulated (Figure 6D). Together, these data argue that glycolysis regulates Wnt signaling in the posterior PSM/tail bud of the chicken embryo.

Wnt and FGF signaling are known to mutually regulate each other in the PSM (Aulehla and Pourquie, 2010; Naiche et al., 2011). Accordingly, embryos treated with the FGF/MAPK inhibitor PD0325901 also stopped elongating and showed reduced phosphorylated MAPK and Wnt activity (Figures 7A–7I and 7O–7Q). Glycolysis inhibition also strongly reduced expression of markers of Wnt activation such as *AXIN2* (Figure 7M) as well as targets of FGF signaling such as phosphorylated MAPK and *SPROUTY2* (Figures 7F, 7G, 7M, and 7N). Since *Wnt3a* in the PSM controls *Fgf8* expression in the mouse embryo (Aulehla et al., 2003), our data support the existence of a closed regulatory loop linking FGF and Wnt signaling via glycolysis in the PSM. From these results we conclude that glycolysis downstream of FGF signaling is required to maintain the Wnt gradient in the

(O–T) SOX2 (O and R) and T/BRACHYURY (P and S) protein expression in control (O–Q) and 2DG-treated (R–T) 2-day-old chicken embryos (n = 4 for each condition). (Q and T) Higher magnification of the tail bud stained with SOX2 and T/BRACHYURY. Stippled line delineates the double-positive cells in the chordoneural hinge region. Left panel shows schematic representation of the posterior part of a 2-day-old chicken embryo indicating the position of the sections shown in O–T (axial red dotted line).

(U–Z) Expression of CMESPO (U and X) and CTNNB1 (β-catenin) (V–W, Y–Z) proteins in sagittal sections of a 2-day-old control (U–W, n = 5), and a 2DG-treated (X–Z, n = 4) chicken embryo. (W–Z) Higher magnification of the regions boxed in red in (V) and (Y) showing the nuclear localization of β-CATENIN. Top panel shows anterior PSM. Nuclei labeled with DAPI are shown in blue. Left panel shows a schematic representation of the posterior part of a 2-day-old chicken embryo indicating the position of the sections shown in (U) to (Z) (paraxial blue dotted line).

Scale bars, 100 μm (A–C, E–T, U–V, X–Y) and 10 μm (W, Z). Asterisk indicates newly formed somites and arrowheads indicate tail bud region.

See also Figure S5 and Movie S5.

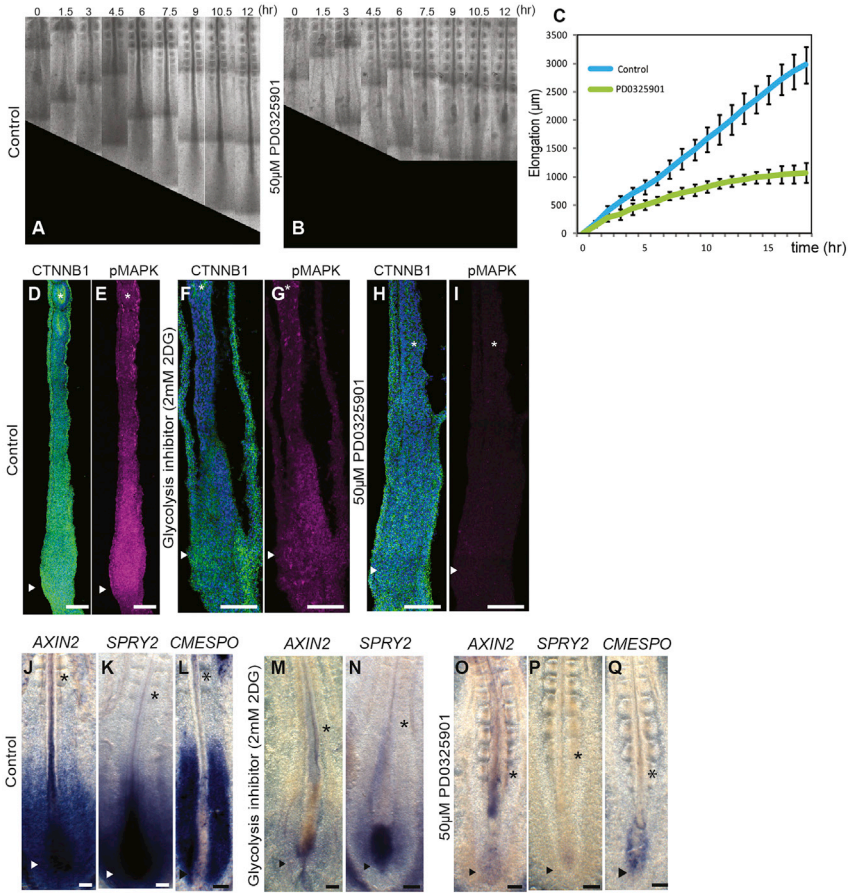

Figure 7. Phenotypic Correlation between FGF and Glycolysis Inhibition

(A and B) Micrographs taken at 1.5-hr intervals of the posterior region of 2-day-old chicken embryo control (A) and treated with PD0325901 (B).

(C) Graph showing the increase in axis length (elongation) measured using time-lapse microscopy in 2-day-old chicken control embryos (blue) and PD0325901-treated embryos (green). Data represent the average of five embryos per condition; error bars denote mean ± SD.

(D–I) Expression of CTNNB1 (β-catenin) (green, D, F, H) and phosphorylated MAPK (magenta, E, G, I) in longitudinal sections of control (D, E; n = 5), 2DG-treated (F, G; n = 4), and PD0325901-treated (H, I: n = 4) 2-day-old chicken embryos. Sections shown in (D), (F), and (H) are counterstained with DAPI (in blue) to visualize the nuclei.

(J–Q) Expression of *AXIN2* (J, M, O), *SPRY2* (K, N, P), and *CMESPO* (L, Q) detected by whole-mount in situ hybridization in the posterior part of 2-day-old chicken control embryos (J, n = 5; K, n = 5; L, n = 4), 2DG-treated embryos (M, n = 4; N, n = 3), and PD0325901-treated embryos (O, n = 4; P, n = 3; Q, n = 4).

Scale bars, 100 μm. Ventral view, anterior to the top. Asterisks indicate newly formed somites and arrowheads indicate tail bud region.

posterior PSM. In turn, the Wnt gradient is required to maintain FGF activation.

Conclusion

Our study shows that glycolysis acts independently of energy production in specific developmental processes that are necessary to sustain posterior elongation of the embryonic axis: the Wnt-dependent production of paraxial mesoderm cells from tail bud NMPs and the control of their motility. How glycolysis regulates Wnt signaling remains to be established. In yeast and cancer cells, glycolysis regulates intracellular pH, which in turn controls V-ATPase assembly (Dechant et al., 2010). The recent implication of V-ATPase in Wnt signaling might provide a link between glycolysis and Wnt in the embryo (Cruciat et al., 2010). The effect on cell motility might be linked to the role of localized glycolytic activity, ensuring rapid delivery of ATP for actin polymerization to the forming protrusions, which was hypothesized in cancer or endothelial cells (De Bock et al., 2013; Nguyen et al., 2000).

Our data are corroborated by a companion study that used a different set of approaches to identify a similar gradient of glycolytic activity in the posterior PSM of mouse embryos (Bulusu et al., 2017). Using metabolic labeling, this study demonstrated an increase in the glycolytic flux in the posterior PSM of mouse embryos. The striking similarities between the embryonic metabolic state described in these two reports and the Warburg metabolism suggest that cancer cells could redeploy a specific embryonic metabolic program with significant consequences on cell signaling and proliferation. Strikingly, however, the increased aerobic glycolysis observed in the tail bud and posterior PSM does not appear to correlate with an increased proliferation rate, supporting different roles for this type of metabolism such as coordinating cell signaling.

STAR★METHODS

Detailed methods are provided in the online version of this paper and include the following:

- KEY RESOURCES TABLE
- CONTACT FOR REAGENT AND RESOURCE SHARING
- EXPERIMENTAL MODEL AND SUBJECT DETAILS
  - Animals
  - Chicken Embryo Culture
- METHOD DETAILS
  - Mouse Embryos Dissection and Metabolome Analysis
  - Chicken Embryo PSM Microdissection and Microarray
  - Measurement of Metabolic Activity
  - Time-Lapse Imaging and Axis Elongation Measurement
  - Whole Mount In Situ Hybridization
  - CMESPO Antibody Generation
  - Immunohistochemistry
  - Plasmid Preparation and Electroporation
  - Cell Proliferation and Apoptosis Analysis
  - Quantitative RT-PCR
  - Glucose Uptake

- Image Acquisition and Processing
- Extracellular pH Measurement
- QUANTIFICATION AND STATISTICAL ANALYSIS
  - Cell Trajectory Analysis
  - Metabolome Statistical Analysis
  - Other Statistical Analyses
- DATA AND SOFTWARE AVAILABILITY

SUPPLEMENTAL INFORMATION

Supplemental Information includes five figures, three tables, and five movies and can be found with this article online at http://dx.doi.org/10.1016/j.devcel.2017.02.001.

AUTHOR CONTRIBUTIONS

M.O. designed, performed, and analyzed the experiments with O.P. E.K. supervised the metabolomic analysis. P.M. analyzed the microarray data. J.C. generated the anti-CMESPO antibody. K.G. and F.X. analyzed the imaging data. M.O. and O.P. wrote the manuscript, and O.P. supervised the project. All authors discussed and agreed on the results and commented on the manuscript.

ACKNOWLEDGMENTS

We thank members of the Pourquié laboratory and Michel Labouesse, Norbert Perrimon, Alexander Aulehla, Ralph DeBerardinis, and Cliff Tabin for discussions and comments on the manuscript. We are grateful to Bertrand Bénazéraf, Alexis Hubaud, Nicolas Denans, and Aurélie Krol for assistance with some chicken embryo experiments. We thank members of IGBMC imaging and microarray facility and Jean Marie Garnier for plasmid construction. This work was supported by an advanced grant of the European Research Council (249931) to O.P., an NIH RO1 grant 11955884 to O.P., and a grant of the Fondation pour la Recherche Médicale (SPF20120523860) to M.O. F.X. was supported by an HHMI-HHWF fellowship. E.D.K. is an employee of Metabolon Inc., a fee-for-service metabolomics provider. This work was partially supported by the French Agence Nationale pour la Recherche under grant ANR-14-CE32-0009-01 to K.G.

Received: August 22, 2016
Revised: November 23, 2016
Accepted: January 31, 2017
Published: February 27, 2017

REFERENCES

Agathocleous, M., Love, N.K., Randlett, O., Harris, J.J., Liu, J., Murray, A.J., and Harris, W.A. (2012). Metabolic differentiation in the embryonic retina. Nat. Cell Biol. *14*, 859–864.

Aulehla, A., and Pourquie, O. (2010). Signaling gradients during paraxial mesoderm development. Cold Spring Harb. Perspect. Biol. *2*, a000869.

Aulehla, A., Wehrle, C., Brand-Saberi, B., Kemler, R., Gossler, A., Kanzler, B., and Herrmann, B.G. (2003). Wnt3a plays a major role in the segmentation clock controlling somitogenesis. Dev. Cell *4*, 395–406.

Aulehla, A., Wiegraebe, W., Baubet, V., Wahl, M.B., Deng, C., Taketo, M., Lewandoski, M., and Pourquie, O. (2008). A beta-catenin gradient links the clock and wavefront systems in mouse embryo segmentation. Nat. Cell Biol. *10*, 186–193.

Benazeraf, B., and Pourquie, O. (2013). Formation and segmentation of the vertebrate body axis. Annu. Rev. Cell Dev. Biol. *29*, 1–26.

Benazeraf, B., Francois, P., Baker, R.E., Denans, N., Little, C.D., and Pourquie, O. (2010). A random cell motility gradient downstream of FGF controls elongation of an amniote embryo. Nature *466*, 248–252.

Brinster, R.L. (1965). Studies on the development of mouse embryos in vitro. Ii. The effect of energy source. J. Exp. Zool. *158*, 59–68.

Buchberger, A., Seidl, K., Klein, C., Eberhardt, H., and Arnold, H.H. (1998). cMeso-1, a novel bHLH transcription factor, is involved in somite formation in chicken embryos. Dev. Biol. *199*, 201–215.

Buchberger, A., Bonneick, S., and Arnold, H. (2000). Expression of the novel basic-helix-loop-helix transcription factor cMespo in presomitic mesoderm of chicken embryos. Mech. Dev. *97*, 223–226.

Bulusu, V., Prior, N., Snaebjornsson, M.T., Kuehne, A., Sonnen, K., Kress, J., Stein, F., Schultz, C., Sauer, U., and Aulehla, A. (2017). Spatiotemporal analysis of a glycolytic activity gradient linked to mouse embryo mesoderm development. Dev. Cell *40*, this issue, 331–341.

Chal, J., Oginuma, M., Al Tanoury, Z., Gobert, B., Sumara, O., Hick, A., Bousson, F., Zidouni, Y., Mursch, C., Moncuquet, P., et al. (2015). Differentiation of pluripotent stem cells to muscle fiber to model Duchenne muscular dystrophy. Nat. Biotechnol. *33*, 962–969.

Chapman, D.L., and Papaioannou, V.E. (1998). Three neural tubes in mouse embryos with mutations in the T-box gene Tbx6. Nature *391*, 695–697.

Chapman, S.C., Collignon, J., Schoenwolf, G.C., and Lumsden, A. (2001). Improved method for chick whole-embryo culture using a filter paper carrier. Dev. Dyn. *220*, 284–289.

Clough, J.R., and Whittingham, D.G. (1983). Metabolism of [14C]glucose by postimplantation mouse embryos in vitro. J. Embryol. Exp. Morphol. *74*, 133–142.

Crossley, P.H., and Martin, G.R. (1995). The mouse Fgf8 gene encodes a family of polypeptides and is expressed in regions that direct outgrowth and patterning in the developing embryo. Development *121*, 439–451.

Cruciat, C.M., Ohkawara, B., Acebron, S.P., Karaulanov, E., Reinhard, C., Ingelfinger, D., Boutros, M., and Niehrs, C. (2010). Requirement of prorenin receptor and vacuolar H+-ATPase-mediated acidification for Wnt signaling. Science *327*, 459–463.

Dale, J.K., Maroto, M., Dequeant, M.L., Malapert, P., McGrew, M., and Pourquie, O. (2003). Periodic notch inhibition by lunatic fringe underlies the chick segmentation clock. Nature *421*, 275–278.

De Bock, K., Georgiadou, M., Schoors, S., Kuchnio, A., Wong, B.W., Cantelmo, A.R., Quaegebeur, A., Ghesquiere, B., Cauwenberghs, S., Eelen, G., et al. (2013). Role of PFKFB3-driven glycolysis in vessel sprouting. Cell *154*, 651–663.

Dechant, R., Binda, M., Lee, S.S., Pelet, S., Winderickx, J., and Peter, M. (2010). Cytosolic pH is a second messenger for glucose and regulates the PKA pathway through V-ATPase. EMBO J. *29*, 2515–2526.

Dehaven, C.D., Evans, A.M., Dai, H., and Lawton, K.A. (2010). Organization of GC/MS and LC/MS metabolomics data into chemical libraries. J. Cheminform *2*, 9.

Denans, N., Iimura, T., and Pourquie, O. (2015). Hox genes control vertebrate body elongation by collinear Wnt repression. Elife *4*, e04379.

Esen, E., Chen, J., Karner, C.M., Okunade, A.L., Patterson, B.W., and Long, F. (2013). WNT-LRP5 signaling induces Warburg effect through mTORC2 activation during osteoblast differentiation. Cell Metab. *17*, 745–755.

Evans, A.M., DeHaven, C.D., Barrett, T., Mitchell, M., and Milgram, E. (2009). Integrated, nontargeted ultrahigh performance liquid chromatography/electrospray ionization tandem mass spectrometry platform for the identification and relative quantification of the small-molecule complement of biological systems. Anal. Chem. *81*, 6656–6667.

Gardner, D.K. (2015). Lactate production by the mammalian blastocyst: manipulating the microenvironment for uterine implantation and invasion? Bioessays *37*, 364–371.

Gomez, C., Ozbudak, E.M., Wunderlich, J., Baumann, D., Lewis, J., and Pourquie, O. (2008). Control of segment number in vertebrate embryos. Nature *454*, 335–339.

Greco, T.L., Takada, S., Newhouse, M.M., McMahon, J.A., McMahon, A.P., and Camper, S.A. (1996). Analysis of the vestigial tail mutation demonstrates that Wnt-3a gene dosage regulates mouse axial development. Genes Dev. *10*, 313–324.

Hamburger, V., and Hamilton, H.L. (1992). A series of normal stages in the development of the chick embryo (1951). Dev. Dyn. *195*, 231–272.

Henrique, D., Adam, J., Myat, A., Chitnis, A., Lewis, J., and Ish-Horowicz, D. (1995). Expression of a Delta homologue in prospective neurons in the chick. Nature *375*, 787–790.

Henrique, D., Abranches, E., Verrier, L., and Storey, K.G. (2015). Neuromesodermal progenitors and the making of the spinal cord. Development *142*, 2864–2875.

Hubaud, A., and Pourquie, O. (2014). Signalling dynamics in vertebrate segmentation. Nat. Rev. Mol. Cell Biol. *15*, 709–721.

Itoh, Y., Abe, T., Takaoka, R., and Tanahashi, N. (2004). Fluorometric determination of glucose utilization in neurons in vitro and in vivo. J. Cereb. Blood Flow Metab. *24*, 993–1003.

Johnson, M.T., Mahmood, S., and Patel, M.S. (2003). Intermediary metabolism and energetics during murine early embryogenesis. J. Biol. Chem. *278*, 31457–31460.

Kimelman, D. (2016). Tales of tails (and trunks): forming the posterior body in vertebrate embryos. Curr. Top. Dev. Biol. *116*, 517–536.

Krol, A.J., Roellig, D., Dequeant, M.L., Tassy, O., Glynn, E., Hattem, G., Mushegian, A., Oates, A.C., and Pourquie, O. (2011). Evolutionary plasticity of segmentation clock networks. Development *138*, 2783–2792.

McGrew, M.J., Sherman, A., Ellard, F.M., Lillico, S.G., Gilhooley, H.J., Kingsman, A.J., Mitrophanous, K.A., and Sang, H. (2004). Efficient production of germline transgenic chickens using lentiviral vectors. EMBO Rep. *5*, 728–733.

Minowada, G., Jarvis, L.A., Chi, C.L., Neubuser, A., Sun, X., Hacohen, N., Krasnow, M.A., and Martin, G.R. (1999). Vertebrate Sprouty genes are induced by FGF signaling and can cause chondrodysplasia when overexpressed. Development *126*, 4465–4475.

Moussaieff, A., Rouleau, M., Kitsberg, D., Cohen, M., Levy, G., Barasch, D., Nemirovski, A., Shen-Orr, S., Laevsky, I., Amit, M., et al. (2015). Glycolysis-mediated changes in acetyl-CoA and histone acetylation control the early differentiation of embryonic stem cells. Cell Metab. *21*, 392–402.

Naiche, L.A., Holder, N., and Lewandoski, M. (2011). FGF4 and FGF8 comprise the wavefront activity that controls somitogenesis. Proc. Natl. Acad. Sci. USA *108*, 4018–4023.

Nguyen, T.N., Wang, H.J., Zalzal, S., Nanci, A., and Nabi, I.R. (2000). Purification and characterization of beta-actin-rich tumor cell pseudopodia: role of glycolysis. Exp. Cell Res. *258*, 171–183.

Nowotschin, S., Ferrer-Vaquer, A., Concepcion, D., Papaioannou, V.E., and Hadjantonakis, A.K. (2012). Interaction of Wnt3a, Msgn1 and Tbx6 in neural versus paraxial mesoderm lineage commitment and paraxial mesoderm differentiation in the mouse embryo. Dev. Biol. *367*, 1–14.

Ogawa, M., Kosaka, N., Regino, C.A., Mitsunaga, M., Choyke, P.L., and Kobayashi, H. (2010). High sensitivity detection of cancer in vivo using a dual-controlled activation fluorescent imaging probe based on H-dimer formation and pH activation. Mol. Biosyst. *6*, 888–893.

Okada, A., Lansford, R., Weimann, J.M., Fraser, S.E., and McConnell, S.K. (1999). Imaging cells in the developing nervous system with retrovirus expressing modified green fluorescent protein. Exp. Neurol. *156*, 394–406.

Olivera-Martinez, I., Harada, H., Halley, P.A., and Storey, K.G. (2012). Loss of FGF-dependent mesoderm identity and rise of endogenous retinoid signalling determine cessation of body axis elongation. PLoS Biol. *10*, e1001415.

Ozbudak, E.M., Tassy, O., and Pourquie, O. (2010). Spatiotemporal compartmentalization of key physiological processes during muscle precursor differentiation. Proc. Natl. Acad. Sci. USA *107*, 4224–4229.

Papaconstantinou, J. (1967). Metabolic control of growth and differentiation in vertebrate embryos. In The Biochemistry of Animal Development, R. Weber, ed. (Academic Press), pp. 57–113.

Parks, S.K., Chiche, J., and Pouyssegur, J. (2013). Disrupting proton dynamics and energy metabolism for cancer therapy. Nat. Rev. *13*, 611–623.

Primmett, D.R., Norris, W.E., Carlson, G.J., Keynes, R.J., and Stern, C.D. (1989). Periodic segmental anomalies induced by heat shock in the chick embryo are associated with the cell cycle. Development *105*, 119–130.

Qian, H., Sheetz, M.P., and Elson, E.L. (1991). Single particle tracking. Analysis of diffusion and flow in two-dimensional systems. Biophys. J. *60*, 910–921.

Reitman, Z.J., Jin, G., Karoly, E.D., Spasojevic, I., Yang, J., Kinzler, K.W., He, Y., Bigner, D.D., Vogelstein, B., and Yan, H. (2011). Profiling the effects of isocitrate dehydrogenase 1 and 2 mutations on the cellular metabolome. Proc. Natl. Acad. Sci. USA *108*, 3270–3275.

Sbalzarini, I.F., and Koumoutsakos, P. (2005). Feature point tracking and trajectory analysis for video imaging in cell biology. J. Struct. Biol. *151*, 182–195.

Shepard, T.H., Tanimura, T., and Park, H.W. (1997). Glucose absorption and utilization by rat embryos. Int. J. Dev. Biol. *41*, 307–314.

Shyh-Chang, N., Daley, G.Q., and Cantley, L.C. (2013). Stem cell metabolism in tissue development and aging. Development *140*, 2535–2547.

Sparrow, D.B., Chapman, G., Smith, A.J., Mattar, M.Z., Major, J.A., O'Reilly, V.C., Saga, Y., Zackai, E.H., Dormans, J.P., Alman, B.A., et al. (2012). A mechanism for gene-environment interaction in the etiology of congenital scoliosis. Cell *149*, 295–306.

Spratt, N.T., Jr. (1948). Development of the early chick blastoderm on synthetic media. J. Exp. Zool. *107*, 39–64.

Takemoto, T., Uchikawa, M., Yoshida, M., Bell, D.M., Lovell-Badge, R., Papaioannou, V.E., and Kondoh, H. (2011). Tbx6-dependent Sox2 regulation determines neural or mesodermal fate in axial stem cells. Nature *470*, 394–398.

Tzouanacou, E., Wegener, A., Wymeersch, F.J., Wilson, V., and Nicolas, J.F. (2009). Redefining the progression of lineage segregations during mammalian embryogenesis by clonal analysis. Dev. Cell *17*, 365–376.

Vander Heiden, M.G., Cantley, L.C., and Thompson, C.B. (2009). Understanding the Warburg effect: the metabolic requirements of cell proliferation. Science *324*, 1029–1033.

Venters, S.J., Hultner, M.L., and Ordahl, C.P. (2008). Somite cell cycle analysis using somite-staging to measure intrinsic developmental time. Dev. Dyn. *237*, 377–392.

Wales, R.G., Martin, K.L., and Leese, H.J. (1995). Glucose utilization by components of the mouse conceptus during early embryogenesis. J. Reprod. Fertil. *104*, 125–132.

Wittler, L., Shin, E.H., Grote, P., Kispert, A., Beckers, A., Gossler, A., Werber, M., and Herrmann, B.G. (2007). Expression of Msgn1 in the presomitic mesoderm is controlled by synergism of WNT signalling and Tbx6. EMBO Rep. *8*, 784–789.

Yamaguchi, T.P., Takada, S., Yoshikawa, Y., Wu, N., and McMahon, A.P. (1999). T (Brachyury) is a direct target of Wnt3a during paraxial mesoderm specification. Genes Dev. *13*, 3185–3190.

Yoshioka, K., Takahashi, H., Homma, T., Saito, M., Oh, K.B., Nemoto, Y., and Matsuoka, H. (1996). A novel fluorescent derivative of glucose applicable to the assessment of glucose uptake activity of *Escherichia coli*. Biochim. Biophys. Acta *1289*, 5–9.

STAR★METHODS

KEY RESOURCES TABLE

Reagent or Resource	Source	Identifier
Antibodies		
Rabbit polyclonal anti-CMESPO	this paper	N/A
Rabbit anti glut3 (1:300)	Abcam	Cat#ab41525, RRID: AB_732609
Goat anti T/BRACHYURY (1:1000)	R&D Systems	Cat#AF2085, RRID: AB_2200235
Rabbit anti Sox2 (1:1000)	Millipore	Cat#ab5603, RRID: AB_2286686
Mouse anti CTNNB1/b-Catenin (1:500)	BD transduction laboratories	Cat#610153, RRID: AB_397554
Rabbit anti phosphorylated MAPK (1:400)	Cell Signaling Technology	Cat#4370, RRID: AB_2315112
Rabbit anti phospho Histone H3 (1:1000)	Millipore	Cat#06-570, RRID: AB_310177
Chemicals, Peptides, and Recombinant Proteins		
2-Deoxy-D-glucose	Sigma	Cat# D8375
Sodium azide	Sigma	Cat# S8032
SU5402	Sigma	Cat# SML0443
PD 0325901	AXON MEDCHEM BV	Cat# Axon 1408
DAPT	Sigma	Cat# D5942
BMS204493	synthesized by Novalix	N/A
DMEM/F12 w/o glucose medium	USBiological	Cat# D9807-02
Sodium bicarbonate	Sigma	Cat# S5761
Albumin from chicken egg white	Sigma	Cat# A5503
D-glucose	Sigma	Cat# G7021
BactoAgar	BD Bioscience	Cat#214050
2-NDBG	Life technologies	Cat# N13195
pHrodo Red AM Intracellular pH Indicator	Fischer scientific	Cat# P35372
LysoTracker Red DND-99	Fischer scientific	Cat# L7528
Critical Commercial Assays		
ApopTag Red In Situ Apoptosis Detection Kit	Millipore	Cat# S7165
Lactate assay kit	BioVision	Cat# K607-100
ATPlite Luminescence Assay System	Perkin-Elmer	Cat#6016943
Cytochrome c Oxidase assay kit	Sigma	Cat# cytocox1
iTaq Universal SYBR Green Supermix	Bio-Rad	Cat# 172-5122
QuantiFast SYBR Green RT-PCR Kit	Qiagen	Cat# 204154
Deposited Data		
Chicken microarray series	this paper	GSE75798
Mouse microarray series	Chal et al., 2015	GSE39613
Experimental Models: Organisms/Strains		
Mouse: CD1	ICS mouse facility	N/A
Wild type chicken eggs	Charles River	Cat#10100331
GFP chicken eggs	Clemson University, Dr Susan Chapman	N/A
Oligonucleotides		
Primers for GLUT1 (F: AGTACGGAGAGCATTCCCCT, R: CTCAGGAA GGTGGGAAGCTG)	this paper	N/A
Primers for HK1 (F: GAGTTCAAGCTCACCCACGA, R: CTTCTTCAGG CCTGCTTCCA)	this paper	N/A
Primers for G3P (F: GAACTGAGCGGTGGTGAAGA, R:CCACATG GCATCCAAGGAGT)	this paper	N/A

(*Continued on next page*)

Continued

Reagent or Resource	Source	Identifier
Primers for T (F: CGAGGAGATCACAGCTTTAAAAATT, R: TCATTTCTTTCCTTTGCGTCAA)	this paper	N/A
Primers for CMESPO (F:AAAGCCAGTGAGAGGGAGAA, R: GGTG CACTTGAGGGTCTGTA)	this paper	N/A
Primers for SOX2 (F:GCAGAGAAAAGGGAAAAAGGA, R: TTTCCTAGGGAGGGGTATGAA)	this paper	N/A
Primers for SOX1 (F: AGGAGAATCCCAAGATGCAC, R: CTCCGACATCACCTTCCAC)	this paper	N/A
Primers for SAX1 (F:CAGCTTTCACCTACGAGCAG, R: TGGAACC AGATCTTCACCTG)	this paper	N/A
Primers for BETA ACTIN	Qiagen	Gg_ACTB_1_SG QuantiTect Primer Assay
Primers for GPI	Qiagen	Gg_GPI_1_SG QuantiTect Primer Assay
Primers for PGK1	Qiagen	Gg_PGK1_1_SG QuantiTect Primer Assay
Primers for PFKP	Qiagen	Gg_PFKP_1_SG QuantiTect Primer Assay
Primers for ENO1	Qiagen	Gg_ENO1_1_SG QuantiTect Primer Assay
Primers for PKM	Qiagen	Gg_PKM2_1_SG QuantiTect Primer Assay
Primers for LDHB	Qiagen	Gg_LDHB_1_SG QuantiTect Primer Assay
Primers for AXIN2	Qiagen	Gg_AXIN2_1_SG QuantiTect Primer Assay
Chicken GLUT1 RNA probe aaggagtgtatgcagaagagccagaccccc cgctccctccttcctcgtttctgtacaagtattaaaaacactcaggagagaagttagga ggctcggaggagacgggacgtgccgcagctggttagacctgggagtcagcaccc aagctgtggaactcatccggggtcttgtcgctctggctcgcacccccctggcggaagc ggtaggcgatctcatcgaaggtccggccctttgtctccggcaccttgaagtaggtgaa gatgaagaagaggactagcagcaccgtgaagatgatgaagacgtaggagccaca gagttgcgcaatgtactggaagcccatgcccacaatgaagttggaggtccagttaga cagcccagcaacagcgaaggcagcaggacgagggccttggctgaacagttctgc cacaataaaccaagggatggggcctggaccaatctcaaagaaggccacgaaccc gaagatggcaacgatgctgaggtaggacatccagggcatttggtccagcagcgtca gagcaatggtcatgagtattgcacaccctgccatccctgccaggccaatgaggtgaa gggtcctgcgtccagctcgctccaccacgaagagcgaaacaacagtgaaagctgta ttcaccaccccagagccaatggtggcgtagacgggctgctccacacctgacttctca aagatgctggtggagtagtagaaaaccgcat	this paper	NCBI:NM_205209.1
Chicken PFKP RNA probe aaagctcctcccacgaagcctcacagcctcaaca aatcttccttcatccatggctttctgtacttcttgagtcatctgcacacactccatcaaaggc agacgaacagcctggtttccagagagggacacaacacaagcaggagtgtctggagt agcttctagaagtgcaagcacagcttctacacccattcggcttgccaaaattctatcaaa agctgaaggagttccacctctctgcacatgacccaagatagttactcgggtgtcaaatcc aagccgctgaaccacaagatccttaaccttctctgatgttataggtttgttgtggcaatcaa tagctccttcagctacaataataatattcagccttttctttcgtgcacggttctctgaaagctt aacacacattgaatcctcccatccttcttctggtgggtattcaggaataaatacccaatctg caccacaagctaaggcactgacaagagctaaatacccacagtgtctccccataacctc cagaacaaatgtcctctgatggctttgtgcagtggtcatgatggcatccacaacttcaatg attctgtgcaaggctgagtcagtacctatggtcatatcagtgccacagaagtcattgtctatg gatccaaccattcccacaatgttaaggtaagcatatttcttaacagcttcttcatcaatcttt cctttctgcgctagttcttctagaagtccactccattcttcacggaacagattggcaccagtt aagctaccatctccaccaatcacacaaagattagtgattcccctccgaaccaagttgtag	this paper	NCBI:NM_001031511.1

(*Continued on next page*)

Continued

Reagent or Resource	Source	Identifier
Chicken PGK1 RNA probe cactatttgtttggccctcccacaacttcaacaaac ttcttaacactttcagggccgcagtccaagcccatccagccagcaggaatgcctgaagc cactgtggcttccccagtctgtgcatgctcatcaaatttgtctgcagtgatgaagtcaact ggcaaggtaatcttcacaccgttcttctctgccttggccatcaggtccttgacaatttttgatc cctcttcatcaaacagcgagttgccaatctgcatgttgtttaacactttgagaaaggtgaatg ccattccaccaccaatgatcatctcgttgaccttatctaacatgttactgatcagctggatct tatcctgaactttagctcctccaagaattgctaagaagggtctctctggactctcaagggc ctttgcaaaataatccagttctttcttcatcaggaagccagcagccttctgaggaagatga acacctaccatggagctgtgagcacgatgggcagttccaaaagcatcattgacataaa catctcccaatttagaaagagaggctctgaaagcctccacttttgcagcatcagctttgatc ttgttccctgaagcatccttccctttccctttcttctacatggaatcggaggttctctagcag gatgacggagccgtttgcaggattagcacaggccttctccacctcaggacca	this paper	NCBI:NM_204985.2
Chicken PKM RNA probe ggcaacatcactgccctcagcgcgggtcgggcgag gtttcttgatcatgctttccaacatctgagtggcacaaatgatgggtttgccagccctgttgc agcgcccaatcatcatcttctgtgcgaggaagacttttcagcagggatctcaatacccag gtcaccacgggccaccataatgccatcgctggcctccatgatctcatcaaacctgcgca caccctcgtgattctcaatcttgctgataatcttgatgtgctttccctttcccctagcaccttcc tgacagcatggacatcagcagctttgcggatgaaggaagcgaacaccatgtccacattc tgctccacgccaaatttcaggtcctgaatgtccttctctgagactgcaggcaggtcgac cgcagcacctgggaggttcactcccttcttactaccaagcatgccaccgttctcaacctca gtcatgacaaagtccttgcctttctccttaaccagcaaggaaatgagaccgtcatccacat agattttgctgcccacatctataactttgatgaggttcttgtagtccacccacagcacattctc atcgcagttctccatgaaggcattgtccagcgtcactttgagagctgcgcccttcttgagct ccacctctgctgtgccacttcccttgatgagtccagttcggatttcaggtccttggtgtccag tgcaatagccacaggt	this paper	NCBI: NM_205469.1
Chicken LDHB RNA probe ttacagatctttaagatctttctggatgctccacaatgtgtc tgcactcttcttcagctgagccacttcatcatccttcagcttttggttgatgacacttgtcaatcca gaggcactcaggacacaaggcaggctcaggaagacatcattctcaatgccatatgtgc cctttaccagtgttgacacagaatgaactcggtacaagttcttcagcattgtctcacagagc tcagcaacgctaagaccaatggcccagttcgtatacccccttgagtctgattacctcataggc actttcaacaacctgcttgtgaacttccttccagttctcgctgtctttgtcagttcccatggcag gattcagctcctggagagaaacacctgccacattaactccgctccaaacagccacactag aatcaccatgttctcctaaaatccagccatggcagctggttgggtggataccaagtctctca gccatcaggtagcggaatctagctgtgtctagattgcagccacttccaatcacacggtgctttg gcaggccactcaacttccatgtgacataggttaatatatccactgggttggaaaccacaa ggatagtgcaattggggctgtatttcacaatctgaggaatgatgaatttgaagacgttcaca ttcctctgaaccaggttgagacgactctccccctcttgctgacgaacacctgcagttacta ccacaatcttggagttggctgtgacagcataatctttgtctgccacaatcttatgagtctgaa ggaacaagctgccatgctgtagatccatcatttctccttttagcttgtcttccaaaacatcaacc agagcaagctcatcacaaagaccttgccgaggatgctgatggcacacgccatccccacc tgcccgaccccccaccacggtgatcttgttgctgggaaccgtgctgcccgcggccacggg ggtgatcagcttctccttcagggtcgccat	this paper	NCBI: NM_204177.2
Chicken FGF8 RNA probe gtgttcatgc acttgttcgt cctctgcctg caagcccagg taactgttca gtccccacctaattttacac agcatgtgag ggagcagagc ctggtgacag atcagctcag ccggcggctcgtgcgcacct accagctgta cagccggacc agcgggaagc acgtgcagat cttggacaacaagaaaatca atgcgatggc cgaggacggg gatgtgcacg ccaagctcat cgtcgagaccgacacctttg ggagccgtgt gcgcatcaaa ggggcggcca cggggttcta catctgcatgaacaagaagg ggaaactgat cggcaagagt aacggcaaag gcaaggactg cgtcttcaccgagatcgtgc tggagaacaa ctacacggcg ctgcagaacg ccaagtacga gggctggtacatggccttca cccgcaaggg ccgcccgcgc aagggctcca agacccggcagcaccaacgcgaggtgcact tcatgaagcg gctccccaag ggccaccaga ccaccgagcc ccaccggcgcttcgagttcc tcaactaccc cttcaaccgc aggagcaaaa ggactcgaaa ctccagcgcc agggtgcgcc catgacgcgt gcccctcggt ggactgacgt tgagacattg tgatagggttac taaaggaa aaaaaaaacc caacggggga tgggggggagg atacgagaac tacatgctct agttgttggt aatgtggggg ttgttctgtt tttaca	Crossley and Martin, 1995	NCBI: U41467.1

(*Continued on next page*)

Continued

Reagent or Resource	Source	Identifier
Chicken AXIN2A RNA probe aggaagcgtgccgccggctcgccgaagtctccaag cctcagaagcaacgatgttcaacctcaaatcagcagagggatcgaaaccactccactgct gtacaggggggaaacacccctttttgcaatgcaagtctaacgacagaagatcacaaagagcc aaagaaactcccggttgttcacacctctcagtctagtgagttggttgtcacctatttcttttgcgg agaagaaattccctacaggaggatgttaaaggcccagagcctgacacttgggcactttaag gagcagctgagcaaaaagggaaattatagatactacttcaaaaaggcaagcgacgagttt gactgcggtgcagtgtttgaagagatctgggaagacgaaacaattctgcccatgtacgaag gaaggattcttgggaaagtagaaaggatcgattgatggcatctgtgtttcttgagaaaatttaagca	Krol et al., 2011	chEST 371a17
Chicken CMESO1 RNA probe Tctcgcctcc aacgtgtcct cctggccatc ccctcctcac tgcgcagcgg cagggacctc tctggacccc cccagtgacc ccatcctgga cacggggctg ctgccgccag actttgtgga tgcagagatg gtcacccagg acatctcagc agatctgctc tctctgctgg aggctctgct cccaacacag ccccaggact gagccatgca ccatcagatg cccacgactt gcaggaccca gggagatatg tgtccccct tggacagctg ggagggtggc gaagacaagg tgcttgaagc ctggatccat gctggccgtg actgtacata atatactgtg actgtacata aaatactgtg actgtacata aataaaccct tttgcccac	Buchberger et al., 1998	NCBI: Y17043.2
Chicken cMESPO RNA probe ggcacgaggg cagccggcag ctccagcttt tgctggcggg cagcaggaat tgcttgtccc gcgcgctcct ccagaatgga caaattgcat gagacgttga taaatatgga agacactttg ggttcggagc actctgtctg cttatcctcc tgggactgga agaacacagc tggggctttc gagctgcact ccgtctcctc tccacacagc ttatccccaa cgccgtcctt cgagtcttac tcctcgtccc catgcccggc ggcggccgag accccatata gcggtggcgg cctggtgggc tacggcctgg tggacttccc cccagcctac ctgcccagcc ctggacaggc ccggctgccc aagggcacca aggtgcggat gtcagcccag cgccggagga aagccagtga gagggagaag ctgcggatga ggaccctggc cgacgcgctg cacacactgc gcaactacct gccgcctgcc tacagccagc ggggacagcc cctcaccaaa atacagaccc tcaagtgcac catcaagtac atcagcgaac tgacggagct cctcaacagt gtcaagaggg cgtagggccc agctggagca cctaccctgg caccccgagg ctctgctgtg gaagagcctc ttaaaaaaag acaacaaaac cagtccaatt tcttctttgt tggagcgtgg tttcatgggg tgacagagga acatgaggga gggagagcga gggttgctgc gtacgtagga cgtgatgctg gaaggtgatg tagggctgcc taaagcctga gctgcaagtt gctgagatgg aagtcttgct ttttgttttt cttatgctcc tgttttgttt gtctttttt gtttatttta atgataagct tctgacaaat tttaaagctg atctgataca aaccagaaag ccatctgaat gtcctaggat ttacatatct gtgttctgac tgatcttctg tttactgcag accacagtaa atccatagct tttaaagtga atttgtaaga agtaacaact aatcgcatat gatttataag tatattgatt tgtaggcact ttaatattag gatgaggagg aacatgttta gctagttcaa gtattactta tttgtctaca tttcctctgt acttgaaaat caagaaaaga agtaatagca agaacttctt tgctcataac aaatgccata ttctgtaaca atgccatagt ctgtgctttg tattacatat ctggtagata agtaaagtct aaaactgacc attaaattct ggaaatgaaa tataaaccaa ctgatcttat atagat	Buchberger et al., 2000	NCBI: AJ292363.1
Chicken SPRY2 RNA probe gacgagagtt cagcacggca gcgggtcaca ggccttgcta caggctcggc gtgacagtgg gaggccgcat ggggagcctg acctgcggga tgtcctgacg cagcaagtcc acatcctgtc cctggaccag atcagagcta tccgcaacac gaatgagtac acagagggac cgacggtggc tccgcggcca ggggtcaagt cagctcctcg ttcagcgagc cagcccaaaa gtgagaggcc ccatggcctg cctgagcatc gccattttgg ccgggttcag cacacgcaaa cacacgcttc tcctcgggca cctctgtccc gctccatcag cacagtcagc acgggctcac ggagcagtac aaggacaagt acgagcagta attcctctga acaaagactt ctaggatcat cttcagggcc agttgctgac gggatagtcc gcatgcagcc caagtctgag ctcaagtcaa gcgagctgaa gccgctgagc aaagaagact tgggagcaca cagctacagg tgtgaggact gtgggaagtg caagtgcaag gagtgcacgt atccaaggac cctcccatcg tgttggatct gtgacaaaca gtgtctttgc tcagcccaaa acgtggtcga ttacgggact tgtgtctgct gtgtgaaggg cctcttctat cactgctcca acgatgatga ggacaactgc gctgacaacc cctgctcttg cagtcagtcg cactgctgca ctaggtggtc agccatgggt gtggtgtccc tcttcctgcc ttgcttgtgg tgttacctgc cagccaaggg ttgccttaag ttgtgccagg gctgttacga ccgggtcaat cggcctgggt gccgctgtaa acactccaac acggtttgct gcaaagttcc cagtgtcccc cccaggaact ttgaaaagcc aacatag	Minowada et al., 1999	NCBI: AF176904.1

(*Continued on next page*)

Continued

Reagent or Resource	Source	Identifier
Chicken LFNG RNA probe ctatttataga gaccaactta aagactttct ataaatacgg ggagaagagg gaggagggct tttccggagc tgtgtgtgca cagcgctgtg gtgtctcccc tgttgtctcc tcctgggctg agcacagaca ccccacaccc tggcacatag cgcttggggg agccttgtgg ctgtccccat atctatgggg ctggaacatc ctcctgcagg tgggtgctgc tgggggctgg agcacctggg atgcttgtgt gtatgtggtg tttcccaacc tggcattgct ctccggtgca atgggagagt gatgggcacc ctaaaaacac aggtgcccct cccaagcact gtcatctgtt gtcccatcgc tctcctgggg aacctaagag tgggatccca ccttcccagg tacagctgga gcaaaaccag tttgggaaac gctgcctggg agcaatgttt gccgtgagcc aaggatgaat gtaacccatt gcaacgaggg ttggggactc cgtgttcccc atatccctct ctctgtgtcc cttgtggggg ggaccagcgg gcagagctgg agctgagcat ttccaacccg aagctgagtg aaaatggccc ataatgggtg cgttgtacat atgttattgc gccagtattt tttttactgt gccttttttat agaaagaaaa agaaaaaaaa aaaacaacaa gaaagctcaa catggagaat tatgtagatt ttaagatgct ttttatacgt tttctgtgga tcggaaaaga agaaaaagac aaacgacctt ctgataatct gtttaagaaa gagaaaaaga gaaaaaattg cgttgtcttg taactatcac ttaccttaa	Dale et al., 2003	NCBI: U91849
Chicken BRACHYURY (T) RNA probe atgggct ccccggagga cgcgggcaag gcgccggcgt accgagtgga ccacctgctg agcgcggtgg agagcgagct gcaggcgggc agcgagaagg gagacccgac ggagcgcgag ctgcgcgtgg cgctggagga cggcgagctg tggctgcgct tcaaggagct caccaacgag atgatcgtca ccaagaacgg caggaggatg ttcccggtgc tgaaggtgag cgtgtcgggg ctggacccca acgccatgta ctccttcctg ctggacttcg tggcggccga cgggcaccgc tggaagtacg tcaacggcga gtgggtgccg ggcggcaagc cggagccgca ggcgcccagc tgcgtctaca tccaccccga ctcgcccaac ttcggcgccc actggatgaa ggcgcccgtc tccttcagca aggtcaagct caccaacaag ctcaacggcg gcgggcagat catgctcaac tccctgcaca agtacgagcc ccgcatccac atcgtgcggg tgggcggccc gcagcggatg atcaccagcc attccttccc cgagacccag ttcactgccg tgacggcgta ccagaacgag gagatcacag ctttgaaaat taaatacaac ccatttgcga aggcatttct tgacgcaaag gaaagaaatg atcacaaaga catgatggag gaagcgggag acaaccagca gtctggatac tcgcagttag gtagttggct tattcccggg gctggggctc tgtgcccacc tgccaatcct cactctcagt ttggagcacc cctgtctctc tcccctgctc acagctgtga aaggtactca ccgctgagga atcaccgttc tgccccctac cccaatccct acacccatag aaacaactca ccaacagctt acactgataa ctcctctgcc tgccttccca tgctccagtc ccatgacaat tggtcctccc tgggagttcc cacacacacg actatgctgc ccatgagcca cagcactggc acagctacca gctccagtca gtacccgaac ttatggtccg tgagtaacag caccatcacc ccggcgcctc agtcaagcgg gatgtccaac ggcctgagct cccagttcct gcgtggctct ccggtgcact acaccgctct cccacatccc gtcactgcca ccacctccac atccccactg tacgatggag gagcacctgc agaccttcct gacagccagt acgatgcctc tgcacacact cggttggcat ccatgtggac gcccatcacc ccaccttcca tgtaa	Denans et al., 2015	NCBI: U67086.1
Recombinant DNA		
Plasmid pCAGG-H2B-Venus	Denans et al., 2015	N/A
Plasmid pCAGG-H2B-RFP	Denans et al., 2015	N/A
Plasmid pCAGG-Gap-GFP	Okada et al., 1999	N/A
Software and Algorithms		
Image J fiji	NIH	https://fiji.sc/
R (Bioconductor package 2.8)		http://bioconductor.org
MATLAB	MathWorks	https://www.mathworks.com/products/matlab.html?s_tid=hp_products_matlab
GraphPad 6	Prism	https://www.graphpad.com/scientific-software/prism/
MeV 4.9	TM4	https://www.decodon.com/files/doc/MeV_Manual_4_0.pdf
Other		
Metabolome analysis	Metabolon Inc.	http://www.metabolon.com/

CONTACT FOR REAGENT AND RESOURCE SHARING

Further information and requests for resources and reagents should be directed to and will be fulfilled by the Lead Contact, Olivier Pourquie (pourquie@genetics.med.harvard.edu).

EXPERIMENTAL MODEL AND SUBJECT DETAILS

Animals

E9.5 mice embryos were obtained from breeding pairs of CD1 female and male by Institut Clinique de la Souris (Strasbourg, France). Fertilized chicken eggs were obtained from commercial sources. GFP-chicken eggs were obtained from Clemson University (McGrew et al., 2004). Eggs were incubated at 38°C in a humidified incubator and embryos were staged following the Hamburger and Hamilton (HH) table (Hamburger and Hamilton, 1992). All animal experiments were performed according to the institutions guidelines (IGBMC).

Chicken Embryo Culture

EC Culture

In this study, we started to culture chicken embryos mainly from stage 9HH at 37°C using the Early Chick (EC) culture system (Chapman et al., 2001). For drug treatments, 2mM 2DG (2-Deoxy-D-glucose; Sigma) and 1mM NaN_3 (sodium azide; Sigma) albumin plates were prepared. For signaling inhibitors, 500μM SU5402 (Sigma), 50μM PD0325901 (AXON MEDCHEM BV), 100μM DAPT (Sigma) or 50μM BMS204493 (synthesized by Novalix) were diluted in PBS, and 100 μl of the inhibitor solution was added under and on top of the embryos. For alkaline plates, 23mM NaOH albumin plates (2 ml) were prepared, so that they reached pH11.0-11.3 (the pH of control albumin plates is 9.4-9.6).

Chemically Defined Culture System

Embryos were prepared and cultured as described above on culture plates which include DMEM/F12 w/o glucose medium (USBiological, D9807-02), 0.12% Sodium bicarbonate (Sigma), 1% chicken ovalbumin (Sigma) and 0.3% BactoAgar (BD Bioscience) adding 0.15% glucose in DMEM-plate.

METHOD DETAILS

Mouse Embryos Dissection and Metabolome Analysis

The posterior end of three hundred day 9.5 CD1 mouse embryos was dissected into three consecutive fragments of roughly equivalent size along the antero-posterior axis as shown in Figure 1A. The most posterior fragment includes the tail bud and the level of the posterior PSM, the next level correspond to the level of the anterior PSM and the most anterior level corresponds to the most posterior somitic region. Embryos were dissected in cold PBS on silicone-covered Petri dishes and frozen by batches of five in liquid nitrogen. Triplicate pools of fragments of each level were created. Samples were then shipped to Metabolon Inc. (Durham, NC, USA) for metabolomics analysis and Metabolomic profiling analysis was performed by Metabolon as described below and in (Evans et al., 2009; Reitman et al., 2011).

Sample Accessioning

Each sample received was accessioned into the Metabolon LIMS system and was assigned by the LIMS a unique identifier that was associated with the original source identifier only. This identifier was used to track all sample handling, tasks, results etc. The samples (and all derived aliquots) were tracked by the LIMS system. All portions of any sample were automatically assigned their own unique identifiers by the LIMS when a new task is created; the relationship of these samples is also tracked. All samples were maintained at -80°C until processed.

Sample Preparation

Samples were prepared using the automated MicroLab STAR® system from Hamilton Company. A recovery standard was added prior to the first step in the extraction process for QC purposes. Sample preparation was conducted using aqueous methanol extraction process to remove the protein fraction while allowing maximum recovery of small molecules. The resulting extract was divided into four fractions: one for analysis by UPLC/MS/MS (positive mode), one for UPLC/MS/MS (negative mode), one for GC/MS, and one for backup. Samples were placed briefly on a TurboVap® (Zymark) to remove the organic solvent. Each sample was then frozen and dried under vacuum. Samples were then prepared for the appropriate instrument, either UPLC/MS/MS or GC/MS.

Ultrahigh Performance Liquid Chromatography/Mass Spectroscopy (UPLC/MS/MS)

The LC/MS portion of the platform was based on a Waters ACQUITY ultra-performance liquid chromatography (UPLC) and a Thermo-Finnigan linear trap quadrupole (LTQ) mass spectrometer, which consisted of an electrospray ionization (ESI) source and linear ion-trap (LIT) mass analyzer. The sample extract was dried then reconstituted in acidic or basic LC-compatible solvents, each of which contained 8 or more injection standards at fixed concentrations to ensure injection and chromatographic consistency. One aliquot was analyzed using acidic positive ion optimized conditions and the other using basic negative ion optimized conditions in two independent injections using separate dedicated columns. Extracts reconstituted in acidic conditions were gradient eluted

using water and methanol containing 0.1% formic acid, while the basic extracts, which also used water/methanol, contained 6.5mM Ammonium Bicarbonate. The MS analysis alternated between MS and data-dependent MS^2 scans using dynamic exclusion. Raw data files are archived and extracted as described below.

Gas Chromatography/Mass Spectroscopy (GC/MS)

The samples destined for GC/MS analysis were re-dried under vacuum desiccation for a minimum of 24 hours prior to being derivatized under dried nitrogen using bistrimethyl-silyl-triflouroacetamide (BSTFA). The GC column was 5% phenyl and the temperature ramp was from 40° to 300°C in a 16 minute period. Samples were analyzed on a Thermo-Finnigan Trace DSQ fast-scanning single-quadrupole mass spectrometer using electron impact ionization. The instrument was tuned and calibrated for mass resolution and mass accuracy on a daily basis. The information output from the raw data files was automatically extracted as discussed below.

Quality Assurance/QC

For QA/QC purposes, additional samples were included with each day's analysis. These samples included extracts of a pool of well-characterized human plasma, extracts of a pool created from a small aliquot of the experimental samples, and process blanks. QC samples were spaced evenly among the injections and all experimental samples were randomly distributed throughout the run. A selection of QC compounds was added to every sample for chromatographic alignment, including those under test. These compounds were carefully chosen so as not to interfere with the measurement of the endogenous compounds.

Data Extraction and Compound Identification

Raw data was extracted, peak-identified and QC processed using Metabolon's hardware and software. These systems are built on a web-service platform utilizing Microsoft's .NET technologies, which run on high-performance application servers and fiber-channel storage arrays in clusters to provide active failover and load-balancing (Dehaven et al., 2010). Compounds were identified by comparison to library entries of purified standards or recurrent unknown entities. Metabolon maintains a library based on authenticated standards that contains the retention time/index (RI), mass to charge ratio (*m/z*), and chromatographic data (including MS/MS spectral data) on all molecules present in the library. Furthermore, biochemical identifications are based on three criteria: retention index within a narrow RI window of the proposed identification, nominal mass match to the library +/- 0.2 amu, and the MS/MS forward and reverse scores between the experimental data and authentic standards. The MS/MS scores are based on a comparison of the ions present in the experimental spectrum to the ions present in the library spectrum. While there may be similarities between these molecules based on one of these factors, the use of all three data points can be utilized to distinguish and differentiate biochemicals. More than 2400 commercially available purified standard compounds have been acquired and registered into LIMS for distribution to both the LC and GC platforms for determination of their analytical characteristics.

Chicken Embryo PSM Microdissection and Microarray

PSM microdissection was performed as described (Chal et al., 2015). Stage 12HH chicken embryos were pinned on a silicon-coated petri dish in PBS. After removing the endoderm and the ectoderm, both the left and right posterior paraxial mesoderm from the same embryo were dissected into 10 pieces each. All the fragments were stored in Trizol (Invitrogen) at −80°C for subsequent RNA extraction. Biotinylated cRNA targets were prepared from total RNA using a double amplification protocol according to the GeneChip® Expression Analysis Technical Manual: Two-Cycle Target Labeling Assay (P/N 701021 Rev.5, Affymetrix, Santa Clara, USA). Following fragmentation, cRNAs were hybridized on GeneChip chicken Genome arrays. Each microarray was then washed and stained on a GeneChip fluidics station 450 and scanned with a GeneChip Scanner 3000 7G. Finally, raw data (.CEL Intensity files) were extracted from the scanned images using the Affymetrix GeneChip Command Console (AGCC) version 3.1. CEL files were further processed with MAS5 and RMA algorithms using the Bioconductor package (version 2.8) available through R (version 2.12.1). Probe sets were filtered based on their expression intensity value (MAS5 value). Fold changes were compared between average of MAS values of each fragment for mouse triplicate microarray series (Chal et al., 2015) or chicken duplicate microarray series. Statistical comparisons were performed with unpaired two-tailed student t-test. Microarray data were deposited in GEO database under the accession number of GEO: GSE39613 for Mouse and GEO: GSE75798 for chicken samples.

Measurement of Metabolic Activity

The posterior end of day 9.5 CD1 mouse embryos and stage 11 HH chicken embryos were dissected into 3 parts corresponding to the levels of the posterior PSM (P-PSM), the anterior PSM (A-PSM) and the newly formed somites in cold PBS using tungsten needles (Figure 1A). For each analysis, fragments of the same level from 3 embryos were immediately frozen in liquid nitrogen and pooled. Whole cell lysates were prepared by pipetting and vortexing in *PBS* containing 0.5% Tween 20 and protease inhibitor cocktails (Roche). Each sample was normalized by measuring total protein levels using Bio-Rad protein assay kit (Bio-Rad). To analyze the effect of drugs on metabolic activity, stage 9 HH chicken embryos were incubated at 37°C with inhibitors in EC culture as described above. After 10 h of incubation, the posterior end of treated embryos was dissected and samples were prepared as described above. For chemically defined culture system, after 6h of incubation on culture plates which include DMEM/F12 w/o glucose medium, the posterior end of embryos was dissected and samples were prepared as described above. Cellular lactate levels were measured using a Lactate assay kit (biovision) in accordance with the manufacturer's instructions. Cellular ATP levels were measured using ATPlite Luminescence ATP Detection Assay System (Perkin-Elmer) in accordance with the manufacturer's instructions. Cytochrome-C oxidase activity was measured using CytoCHROME C oxidase assay kit (Sigma) in accordance with the manufacturer's

instructions. Biological triplicates of the experiments were performed, and experiments were reproduced at least twice for each measurement of metabolic activity. Values obtained for these assays were normalized by P-PSM or by control values to compare the different AP levels.

Time-Lapse Imaging and Axis Elongation Measurement

Stage 9HH chicken embryos were cultured ventral side up on a microscope stage using a custom built time-lapse station (Benazeraf et al., 2010). We used a computer controlled, wide-field (10× objective) epifluorescent microscope (Leica DMR) workstation, equipped with a motorized stage and cooled digital camera (QImaging Retiga 1300i), to acquire 12-bit grayscale intensity images (492 × 652 pixels). For each embryo, several images corresponding to different focal planes and different fields were captured at each single time-point (frame). The acquisition rate used was 10 frames per hour (6 min between frames). To quantify axis elongation length, the image sequence was first registered to the last formed somite at the beginning of the time-lapse experiment (yellow asterisk in Figure 3), and the advancement of the Hensen's Node was tracked as a function of time using the manual tracking plug-in in Image J (Denans et al., 2015).

Whole Mount In Situ Hybridization

Stage 9HH embryos were cultured with and without drugs at 38°C in EC culture. After 16 h of incubation with 2DG, 10hr incubation with PD035901 embryos or 6h culture on alkaline plate (pH11) were fixed in 4% paraformaldehyde (PFA). Whole mount in situ hybridization was carried out as described (Henrique et al., 1995). Briefly, formaldehyde-fixed embryos were treated with protease and refixed with 4% formaldehyde/0.1% glutaraldehyde. Hybridization with DIG-labelled RNA probes was performed under stringent conditions (1.3 X SSC, 50% formamide at 65°C, pH5) in a buffer containing 0.2% Tween-20 and 0.5% CHAPS. Washed embryos were treated with Boehringer blocking reagent and incubated overnight in alkaline phosphatase-coupled anti-DIG antibody. After extensive washes, embryos were stained from 30 minutes to 16 hours. Probes for *FGF8* (Crossley and Martin, 1995), *AXIN2* (Krol et al., 2011), *CMESO1* (Buchberger et al., 1998), *CMESPO* (Buchberger et al., 2000), *SPRY2* (Minowada et al., 1999), *L-fng* (Dale et al., 2003) and *BRACHYURY* (Denans et al., 2015) have been described. Probes for *GLUT1*, *PFKP*, *PGK1*, *PKM*, *LDHB* were generated from chicken embryo cDNA by PCR using published sequences (NCBI).

CMESPO Antibody Generation

cDNA coding for the full length chicken CMESPO was cloned in pET vector expression system (Novagen), expressed in *E.coli*. The recombinant protein was purified with His-Bind Kit (Novagen) and used to immunize rabbits (Cocalico Biologicals, Inc.). Sera were collected, assayed and validated by immunohistochemistry and used as anti-CMESPO/MESOGENIN1 polyclonal antibody.

Immunohistochemistry

For whole mount immuno-histochemistry, 9.5 day CD1 mouse embryos and stage 12HH chicken embryos were fixed in 4% paraformaldehyde (PFA) at 4°C overnight. Embryos were incubated with an antibody against Glut3 (1/300, Abcam) at 4°C overnight, and next with secondary antibodies conjugated with AlexaFluor (Molecular probes) at 4°C overnight. Images were captured using a laser scanning confocal microscope (*TCS LSI*; *Leica*) *for Glut3 staining*.

For histological analysis, stage 9HH chicken embryos cultured with or without 2DG for 16h were fixed in 4% PFA. Embryos were then embedded in OCT compound and frozen in liquid nitrogen. Frozen sections (20μm) were incubated overnight at 4°C with the primary antibody, and after washing they were incubated overnight at 4°C with the secondary antibody conjugated with AlexaFluor (Molecular probes). We used antibodies against T/BRACHYURY (1/1000, R&D Systems: AF2085), SOX2 (1/1000, Millipore: ab5603), CTNNB1/β-Catenin (1/500, BD transduction laboratories: #610153): For CTNNB1 staining, antigen retrieval (Incubation with Target Retrieval Solution Citrate pH6 (DAKO) at 105°C for 10min) was needed before first antibody incubation. The BRACHYURY and SOX2 staining images were captured using a laser scanning confocal microscope with a 40X objective (TCS SP5; Leica). To image the whole PSM, we used the tiling and stitching function of the microscope (3 by 2 matrix). *For CMESPO and CTNNB1 stainings*, *images were captured using a laser scanning confocal microscope with a 20X objective* (*TCS SP5*; *Leica*). *Whole images were created by tiling the scans of 8 images. High magnification images were captured with a 63X objective*.

Plasmid Preparation and Electroporation

pCAGG-H2B-Venus and pCAGG-H2B-RFP have been described (Denans et al., 2015). Chicken embryos ranging from stage 6HH to stage 7HH were prepared for EC culture. A DNA solution (1.0-5.0 μg/μl) was microinjected in the space between the vitelline membrane and the epiblast surrounding the anterior primitive streak level, which contains the precursors of the paraxial mesoderm. In vitro electroporations were carried out with five successive square pulses of 8V for 50ms, keeping 4mm distance between anode and cathode using Petri dish type electrodes (CUY701P2, Nepa Gene, Japan) and a CUY21 electroporator (Nepa Gene, Japan). This procedure only labels the superficial epiblast layer. For time-lapse analysis, after electroporation, embryos were re-incubated in a humidified incubator until they reached stage 9HH at 38°C, then embryos were transferred to the microscope stage for time-lapse imaging.

Cell Proliferation and Apoptosis Analysis

Stage 9 HH chicken embryos were cultured on agar plates containing 2DG or NaN_3 at 38°C for 12 h. Embryos were fixed in 1% PFA at 4°C for 20min. Whole mount TUNEL staining was performed using the ApopTag Red In Situ kit (#S7165; Millipore), and proliferating cells were stained using anti-Phospho-histone H3 (pH3) antibody (1/1000, Millipore). For the chemically defined culture system (in Figure S3), stage 11HH chicken embryos were cultured on culture plates which include DMEM/F12 w/o glucose medium (with LysoTracker Red DND-99 (1/500, Fischer scientific) diluted in PBS for detecting apoptotic cells), after 3hr culture embryos were fixed in 4% PFA 4°C for 20min. Apoptotic cells were stained by LysoTracker Red and proliferating cells were stained as described above. Images were captured using a laser scanning confocal microscope (TCS SP5; Leica). Ratios of proliferating and apoptotic cells were calculated by manual counting for DAPI, pH3 and TUNEL positive cells.

Quantitative RT-PCR

Stage 9 HH embryos were cultured with or without 2mM 2DG and PD035901 at 38°C for 10 h. Then total RNA was extracted from dissected tailbud regions. 500ng∼1μg total RNA was used as template for cDNA synthesis using the QuantiTect kit (Qiagen) or Super script III (Thermo Fisher Scientific). RT-PCR was performed using QuantiFast SYBR Green RT-PCR Kit (Qiagen) primers or iTaq Universal SYBR Green Supermix (Bio-Rad) and run on a LightCycler 480II (Roche) or CFX384 Touch qPCR System (Bio-Rad). Beta-Actin was used as an internal control. Data were normalized by control samples.

Glucose Uptake

100μl 1mM 2-NDBG (Life technologies) was added both on top and below stage 11 to 12 HH chicken embryos and incubated at 38°C for 2 h in EC culture. After culture, embryos were fixed in 4% PFA for 20 min, and then washed with PBS for 5 min at least 3 times. Images were captured using a laser scanning confocal microscope (TCS SP5; Leica) or macroscope (*TCS LSI*; *Leica*).

Image Acquisition and Processing

All fluorescent images were acquired on Leica SP5 or *LSI* systems. Images were processed with Imagej Fiji and Adobe Photoshop, and MAX projection images are shown in Figures. Whole mount in situ images were captured on Leica Z16 APOA systems and DFC 420C camera, and Images were processed with Adobe Photoshop. Scale bars were measured using Imagej Fiji for confocal images, and by referencing somite size of control embryos for in situ images.

Extracellular pH Measurement

Stage 9HH embryos were incubated with and without 2DG in EC culture at 38°C for 7 h. Next, embryos were transferred either to control plates (pH 9.6), 2DG-containing plates or alkaline plates (pH 11). Then 100μl 25μM pH sensitive dye (pHrodo Red intracellular pH Indicator: Lifetechnologies) was added both on top and below embryos, which were then incubated at 38°C for 3 h. Embryos were then washed once in PBS, and mounted on MatTek glass-bottom dishes dorsal side up on a thin albumin agar layer (control, 2DG or Alkaline). Images were captured with a laser scanning confocal microscope (TCS SP5; Leica) at 37°C in a humidified atmosphere. In this protocol, pH indicator was mainly trapped on extracellular matrix or cellular membrane regions, indicating that it measures the extracellular pH. After image capture, z-stacks (.lif) of individual embryos were rendered in FluoRender to create maximum projection images centered on the midline of each embryo (cropped to leave ∼400μm on each side of the midline). Intensities were measured on these images using the region of interest (ROI) and plot z-profile functionalities in ImageJ. Unpaired t-tests were applied when comparing average intensities between different experimental conditions. Paired t-tests were applied when comparing between regions the embryo.

QUANTIFICATION AND STATISTICAL ANALYSIS

Cell Trajectory Analysis

To study the motility of cells in the presomitic mesoderm, we analyzed cell trajectories in the posterior region of the PSM in an area of about 400 μm representing 1/3 of the PSM length, as shown schematically with a box in Figures 3G–3I. Because of the small depth of the PSM with respect to its area, the motion of the cells can be considered two dimensional. From the trajectories of cells we obtain their time-averaged displacement, or the mean square displacement, given by: $MSD = \langle \Delta r^2(t) \rangle$, where $\Delta \vec{r}(t) = \vec{r}(t) - \vec{r}(0)$ defines the distance that the cell travels in a time t, known as the lag time. When the diffusive motion in coupled with a drifting flow, the MSD is given by

$$\langle \Delta r^2(t) \rangle = 4Dt + v^2 t^2 \,. \qquad \text{(Equation 1)}$$

where D is the diffusion coefficient and v is the drift, related to the overall movement of the tissue (Qian et al., 1991). For each cell trajectory, the MSD is calculated and adjusted with Equation 1 to obtain D. Cell tracking was performed on fluorescent images using the Mosaic plugin (MOSAIC Group, MPI-CBG, Dresden) for ImageJ (Sbalzarini and Koumoutsakos, 2005). Further analyses to extract D were done using custom made Matlab (MathWorks) routines.

Metabolome Statistical Analysis

Missing values (if any) are assumed to be below the level of detection. However, biochemicals that were detected in all samples from one or more groups but not in samples from other groups were assumed to be near the lower limit of detection in the groups in which they were not detected. In this case, the lowest detected level of these biochemicals was imputed for samples in which that biochemical was not detected. Following log transformation and imputation with minimum observed values for each compound, Welch's two-sample *t*-test was used to identify biochemicals that differed significantly between experimental groups. Pathways were assigned for each metabolite, allowing examination of overrepresented pathways. Hierarchical clustering analysis was performed using Pearson correlation coefficient with the MeV 4.9 (TM4) software.

Other Statistical Analyses

Statistical significance for the comparisons between two groups of data (Table S1 and S2; Figure 3G and 6D), were assessed with unpaired two-tailed student t-test. Statistical significance for multiple groups comparison, (Figures 1E–1G, 2E–2G, 3D–3F, 4A–4C, 4K–4L, and S5), were performed with one-way ANOVA and Tukey multiple comparison tests using GraphPad 6 (Prism).

DATA AND SOFTWARE AVAILABILITY

Chicken embryos microarray data described in this paper have been deposited in GEOMNIBUS under accession code GEO: GSE75798.